Electronic Supplementary Information

Experimental and theoretical study of Tetraphenylethylene-based dicationic compounds for corrosion inhibition of steel and brass in acidic medium

Yiming An[†], Yumeng Chen[†], Xue Lei, Song Gao, Mudi Xin, Fulin Qiao, Yue Zhao, Lushen Zuo, Fei Sun*, Chunlu Wang*

Sinopec Research Institute of Petroleum Processing Co., Ltd. Beijing 100083, P. R. China

*Corresponding authors

E-mail addresses: sunfei.ripp@sinopec.com (Fei Sun)

wcl.ripp@sinopec.com (Chunlu Wang)

Contents

1. Synthesis and characterization

TPE-2NO_2 and TPE-2NH_2 were prepared according to literatures [S1-S5].

Synthesis of TPE-2NH_3·SO_4: In a 50 mL round-bottom flask, TPE-2NH_2 (724 mg, 2.0 mmol) was dissolved in mixed solvent of acetone (15 mL) and ethanol (15 mL). Then, concentrated sulfuric acid (220 mg, 2.2 mmol) was added slowly, with emergence of insoluble sediment immediately. The mixture was stirred for 30 min and filtered. The residue was washed with ethanol for more than three times. Then, it was collected and dried in vacuum, to afford TPE-2NH_3·SO_4 as yellow solid (883 mg) in 96% yield. ^{1}H NMR (400 MHz, DMSO-d_6): δ 7.17 − 7.08 (6 H, m), 7.05 − 6.83 (12 H, m); ^{13}C NMR (100 MHz, DMSO-d_6): δ 146.96, 144.95, 141.78, 135.32, 131.81, 131.07, 130.84, 127.59, 125.43; HRMS (ESI, positive): calcd. for $C_{26}H_{23}N_2$ [M − H^+] (m/z): 363.18558; found: 363.18566.

Synthesis of TPE-2NH_3·2SCN: A suspension of TPE-2NH_3·SO_4 (690 mg, 1.5 mmol) in ethanol (20 mL) was stirred in a 50 mL round-bottom flask. Then, an ethanol (5 mL) solution dissolved with NaSCN (243 mg, 3.0 mmol) was added, heated to 50 °C and stirred for 1 h. After being cooled to room temperature, the mixture was centrifuged and filtered. The organic phase was evaporated and dried in vacuum, to afford TPE-2NH_3·2SCN as yellow solid (670 mg) in 93% yield. ^{1}H NMR (400 MHz, DMSO-d_6): δ 7.20 − 7.11 (6 H, m), 7.10 − 7.03 (8 H, m), 7.01 − 6.95 (4 H, d); ^{13}C NMR (100 MHz, DMSO-d_6): δ 142.76, 141.76, 138.45, 131.99, 131.55, 130.58, 129.78, 128.07, 126.88, 122.00; HRMS (ESI, positive): calcd. for $C_{26}H_{23}N_2$ [M − H^+] (m/z): 363.18558; found: 363.18574. calcd. for $C_{26}H_{22}N_2Na$ [M − 2H^+ + Na^+] (m/z): 385.16752; found: 385.16772.

Synthesis of TPE-2NH_3·2Cl: In a 50 mL round-bottom flask, TPE-2NH_2 (363 mg, 1.0 mmol) was dissolved in mixed solvent of acetone (15 mL) and ethanol (15 mL). Then, concentrated hydrochloric acid (223 mg, 2.2 mmol) was added slowly, with emergence of insoluble sediment immediately. The mixture was stirred for 30 min and filtered. The residue was washed with acetone for more than three times. Then, it was collected and dried in vacuum, to afford TPE-2NH_3·2Cl as yellow solid (413 mg) in 95% yield. ^{1}H NMR (400 MHz, DMSO-d_6): δ 7.18 − 7.11 (6 H, m), 7.09 − 7.01 (8 H, m), 7.00 − 6.95 (4 H, d); ^{13}C NMR (100 MHz, DMSO-d_6): δ 142.75, 141.09, 138.59, 131.73, 130.38, 127.80, 126.54, 120.96; HRMS (ESI, positive): calcd. for $C_{26}H_{23}N_2$ [M − H^+] (m/z): 363.18558; found: 363.18576.

Synthesis of TPE-2NH_3·2Br: In a 50 mL round-bottom flask, TPE-2NH_2 (363 mg, 1.0 mmol) was dissolved in mixed solvent of acetone (15 mL) and ethanol (15 mL). Then, 40% hydrobromic acid (445 mg, 2.2 mmol) was added slowly, with emergence of insoluble sediment immediately. The mixture was stirred for 30 min and filtered. The residue was washed with ethanol for more than three times. Then, it was collected and dried in vacuum, to afford TPE-2NH_3·2Br as yellow solid (498 mg) in 95% yield. ^{1}H NMR (400 MHz, DMSO-d_6): δ 7.20 − 7.11 (6 H, m), 7.10 − 7.03 (8 H, m), 7.01 − 6.95 (4 H, d); ^{13}C NMR (100 MHz, DMSO-d_6): δ 142.71, 141.62, 138.43, 131.89, 130.50, 127.97, 126.77, 121.78; HRMS (ESI, positive): calcd. for $C_{26}H_{23}N_2$ [M − H^+] (m/z): 363.18558; found: 363.18558.

Synthesis of TPE-2NH_3·2NO_3: In a 50 mL round-bottom flask, TPE-2NH_2 (363 mg, 1.0 mmol) was dissolved in mixed solvent of acetone (15 mL) and ethanol (15 mL). Then, concentrated nitric acid (214 mg, 2.2 mmol) was added slowly, with emergence of insoluble sediment immediately. The mixture was stirred for 30 min and filtered. The residue was washed with ethanol for more than three times. Then, it was collected and dried in vacuum, to afford TPE-2NH_3·2NO_3 as brown solid (460 mg) in 94% yield. ^{1}H NMR (400 MHz, DMSO-d_6): δ 7.20 − 7.10 (6 H, m), 7.05 − 6.98 (8 H, m), 6.98 − 6.94 (4 H, d); ^{13}C NMR (100 MHz, DMSO-d_6): δ 142.84, 141.31, 138.60, 131.90, 130.52, 127.96, 126.71, 121.28; HRMS (ESI, positive): calcd. for $C_{26}H_{23}N_2$ [M − H^+] (m/z): 363.18558; found: 363.18536.

Synthesis of TPE-2NH_3·2NH_2SO_3: In a 50 mL round-bottom flask, TPE-2NH_2 (363 mg, 1.0 mmol) was dissolved in mixed solvent of acetone (15 mL) and ethanol (15 mL). Then, sulfamic acid (214 mg, 2.2 mmol) was added slowly, with emergence of insoluble sediment immediately. The mixture was stirred for 30 min and filtered. The residue was washed with ethanol for more than three times. Then, it was collected and dried in vacuum, to afford TPE-2NH_3·2NH_2SO_3 as yellow solid (512 mg) in 92% yield. ^{1}H NMR (400 MHz, DMSO-d_6): δ 7.20 − 7.14 (4 H, m), 7.14 − 7.08 (3 H, m), 7.03 − 6.93 (11 H, m); ^{13}C NMR (100 MHz, DMSO-d_6): δ 146.31, 144.87, 141.65, 135.61, 131.83, 131.57, 130.85, 127.64, 125.52; HRMS (ESI, positive): calcd. for $C_{26}H_{23}N_2$ [M − H^+] (m/z): 363.18558; found: 363.18548.

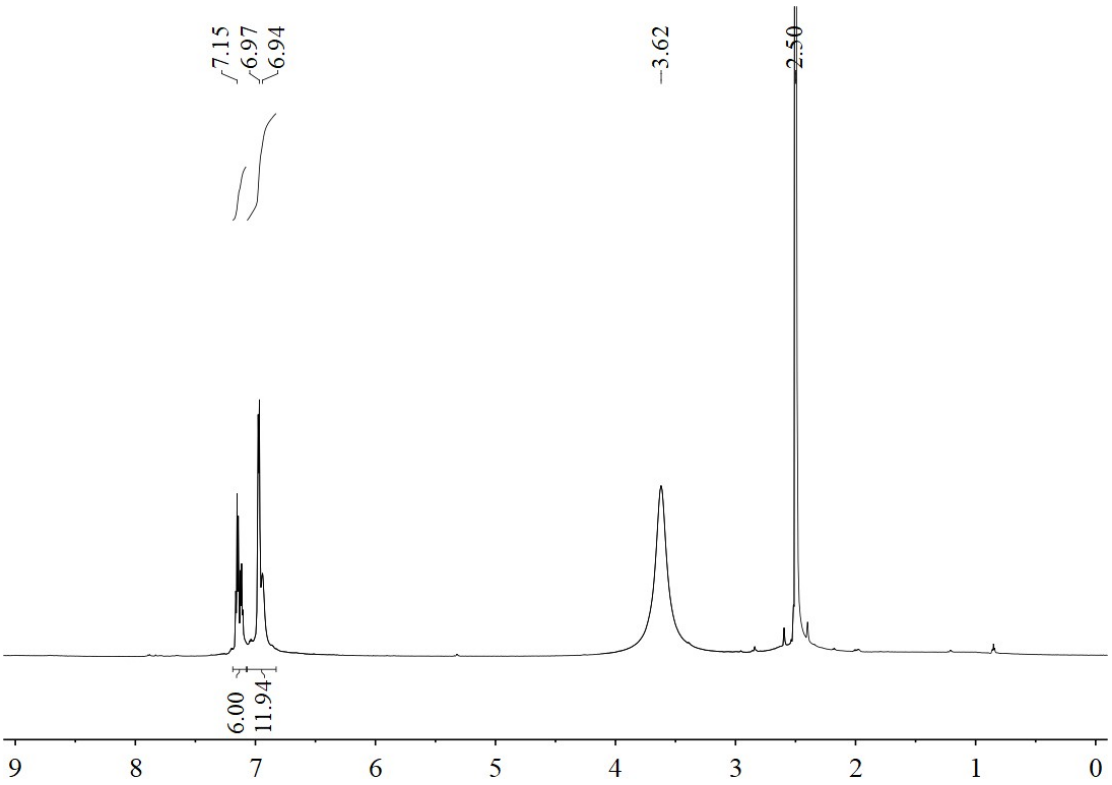

Fig. S1 ^{1}H NMR spectrum of TPE-2$NH_3 \cdot SO_4$.

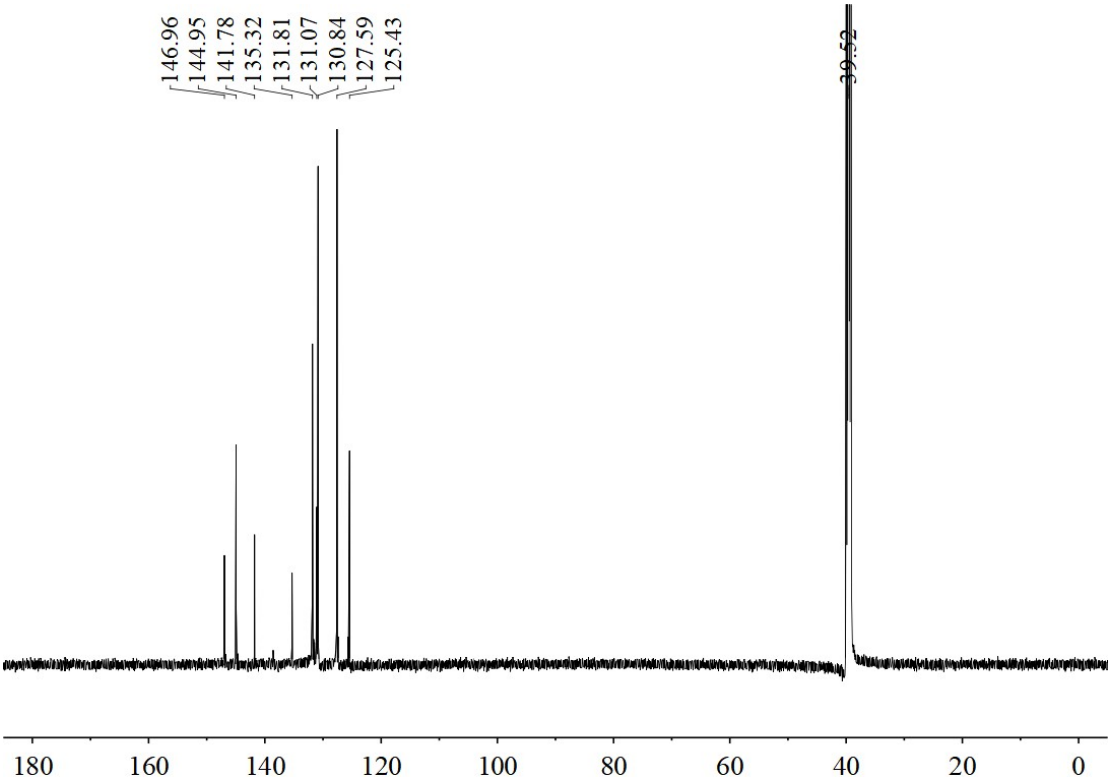

Fig. S2 ^{13}C NMR spectrum of TPE-2$NH_3 \cdot SO_4$.

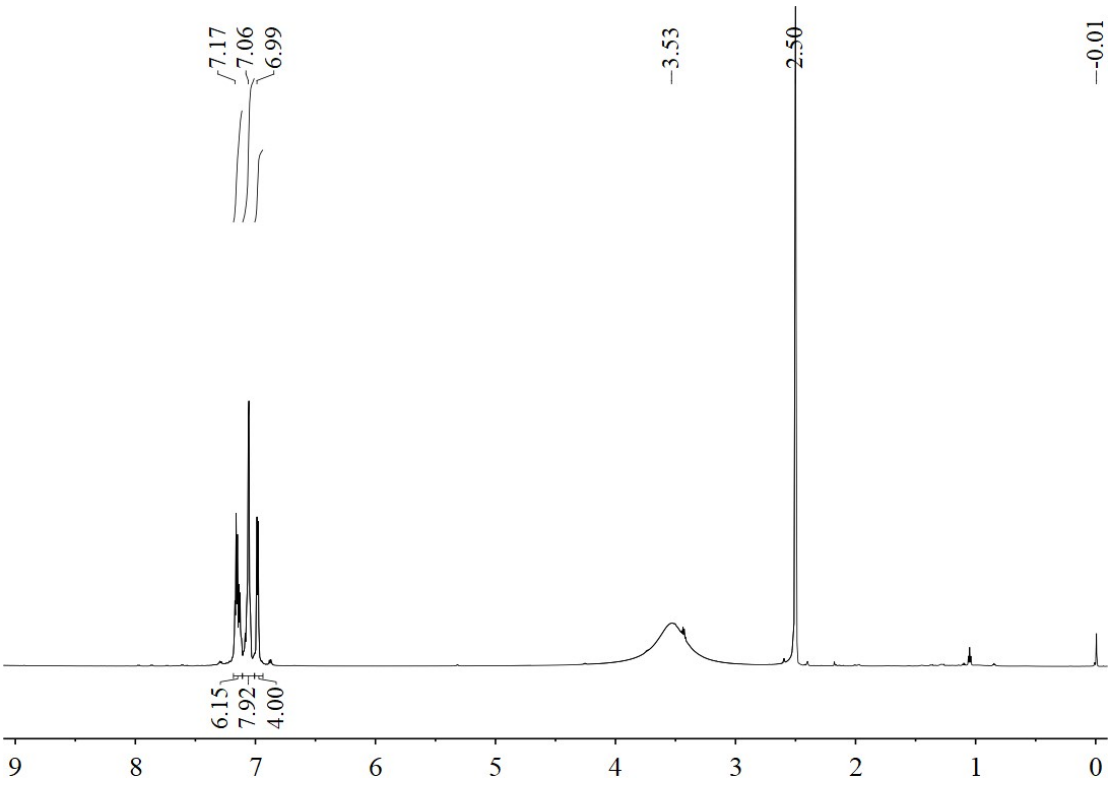

Fig. S3 ^{1}H NMR spectrum of TPE-2NH_3·2SCN.

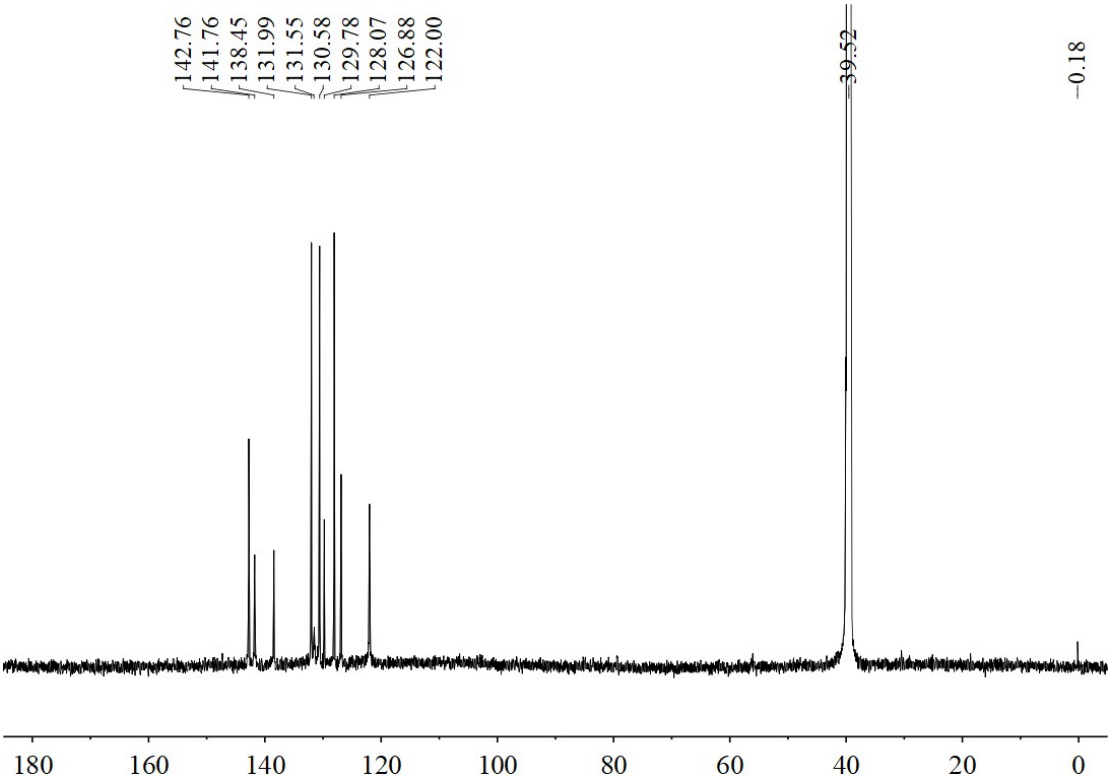

Fig. S4 ^{13}C NMR spectrum of TPE-2NH_3·2SCN.

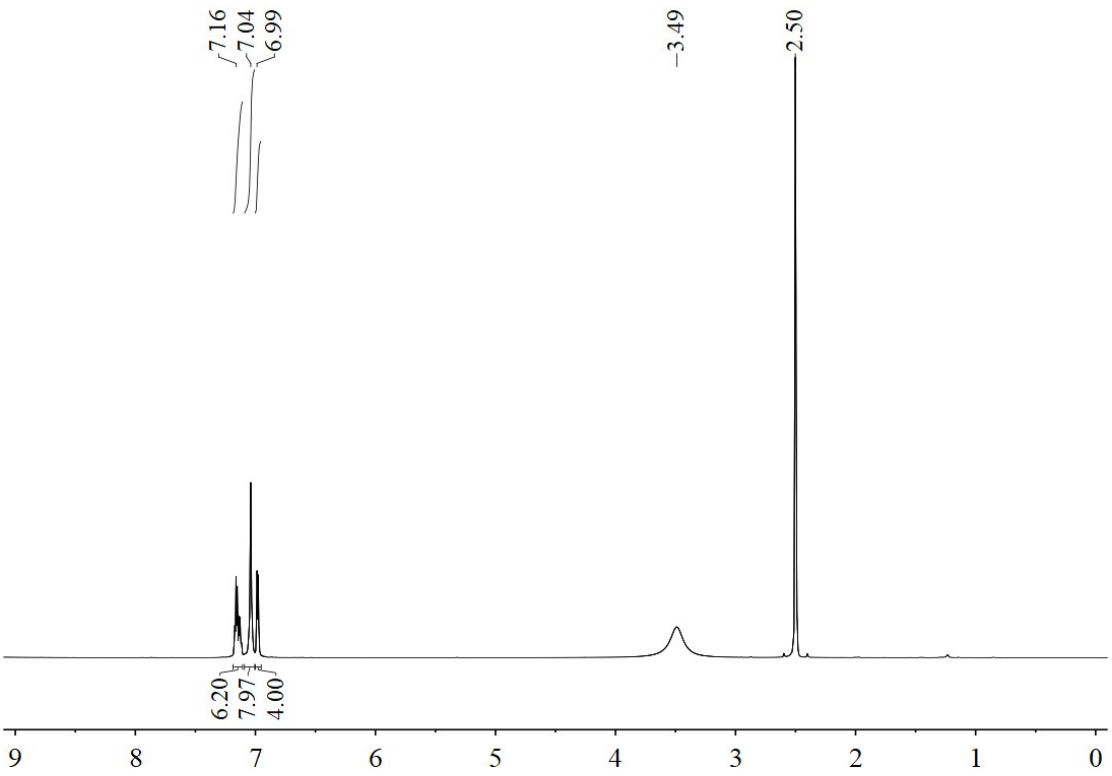

Fig. S5 ^{1}H NMR spectrum of TPE-2NH_3·2Cl.

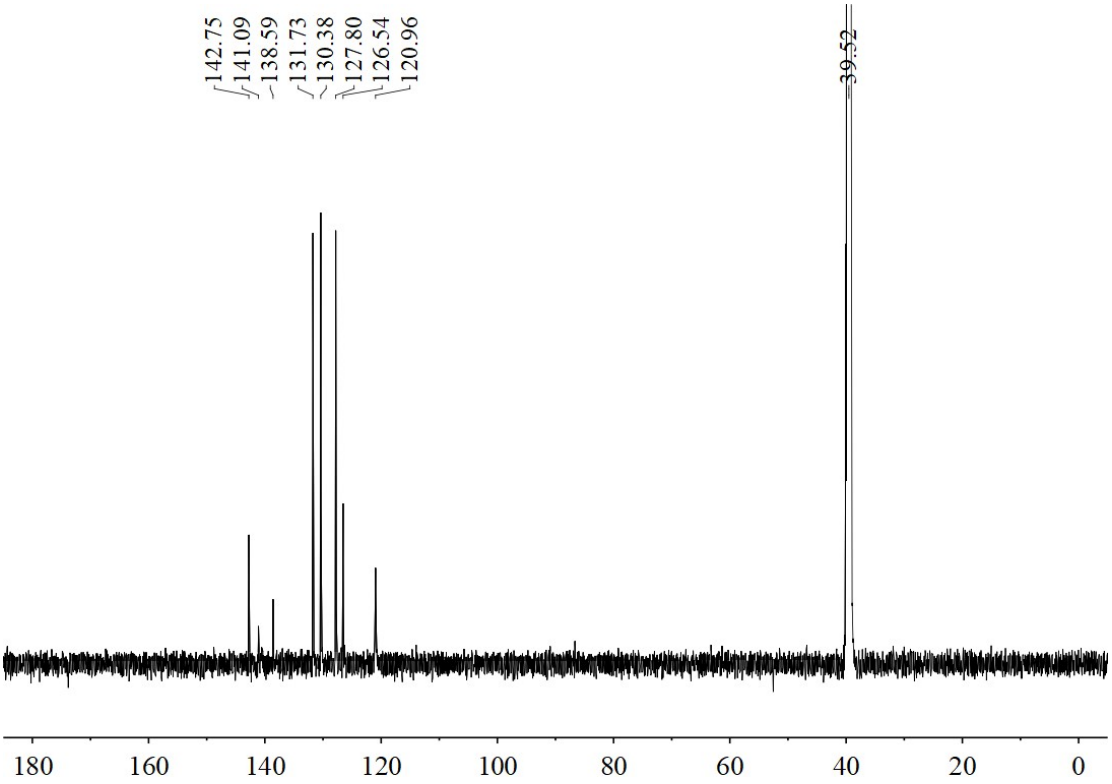

Fig. S6 ^{13}C NMR spectrum of TPE-2NH_3·2Cl.

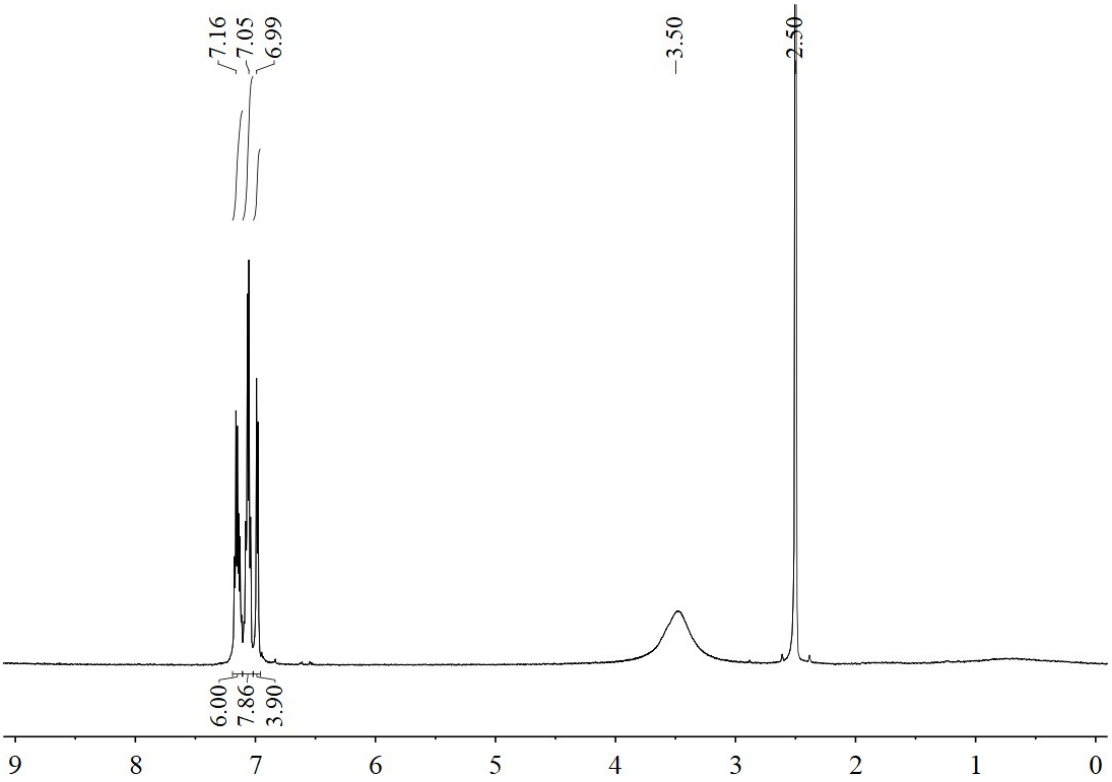

Fig. S7 ^{1}H NMR spectrum of TPE-2NH_3·2Br.

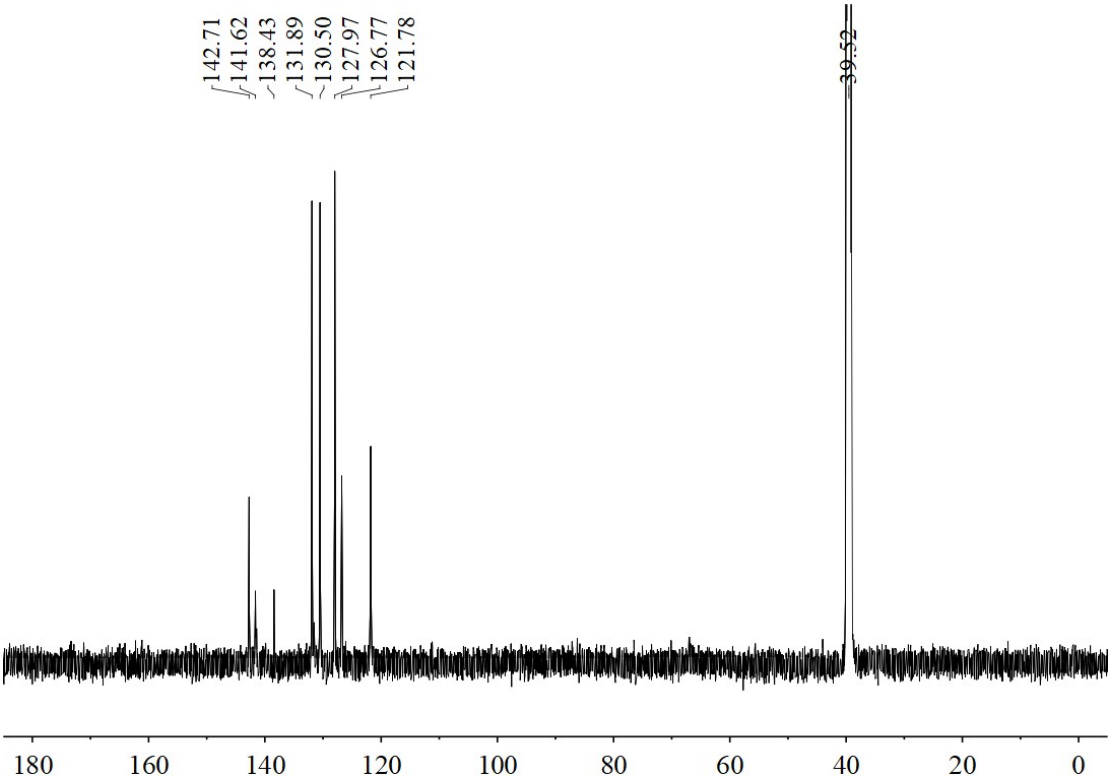

Fig. S8 ^{13}C NMR spectrum of TPE-2NH_3·2Br.

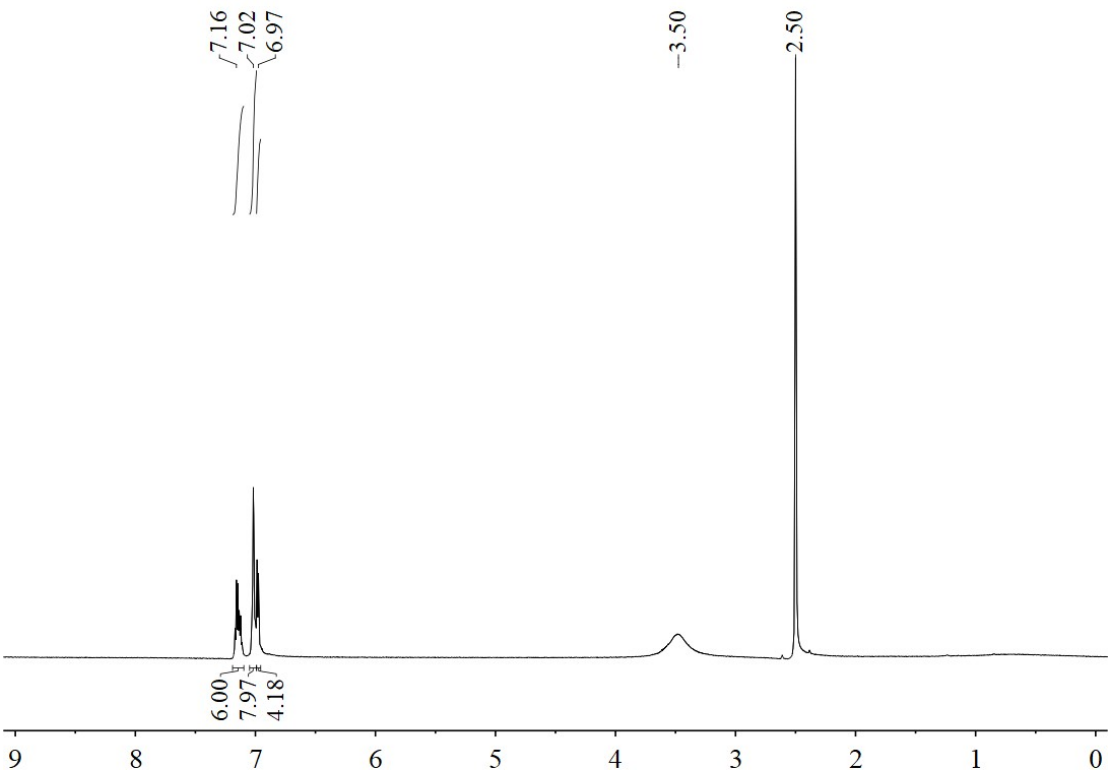

Fig. S9 ^{1}H NMR spectrum of TPE-2NH_3·2NO_3.

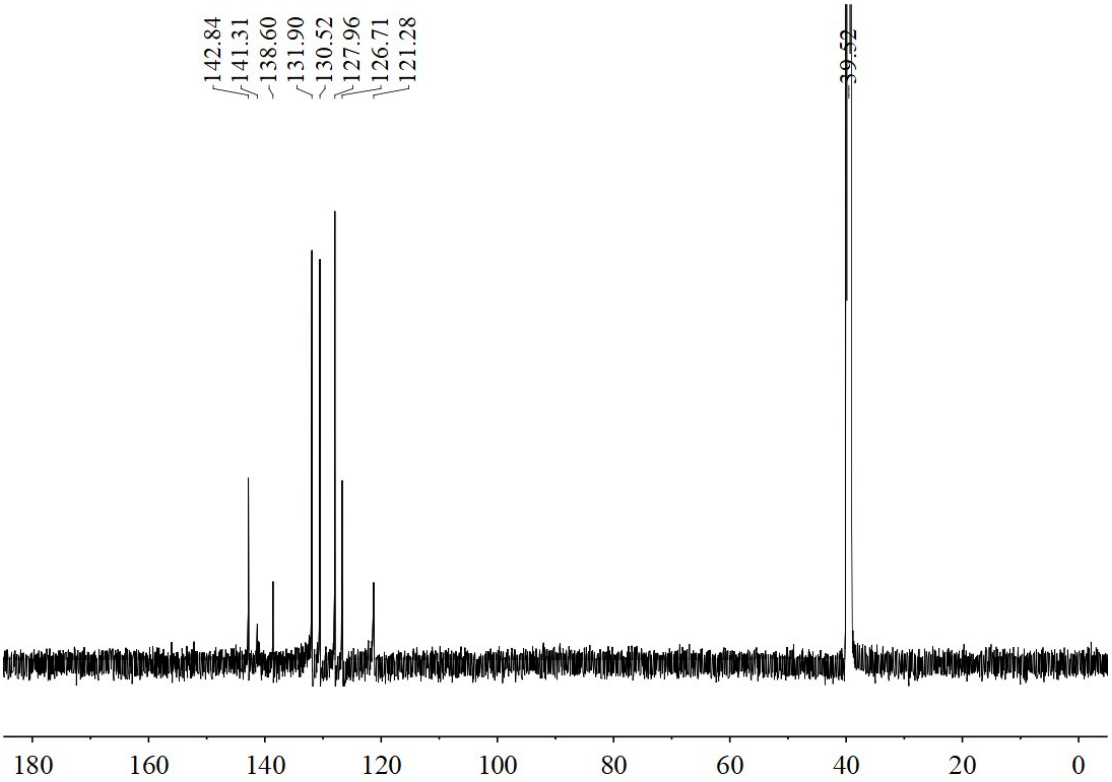

Fig. S10 ^{13}C NMR spectrum of TPE-2NH_3·2NO_3.

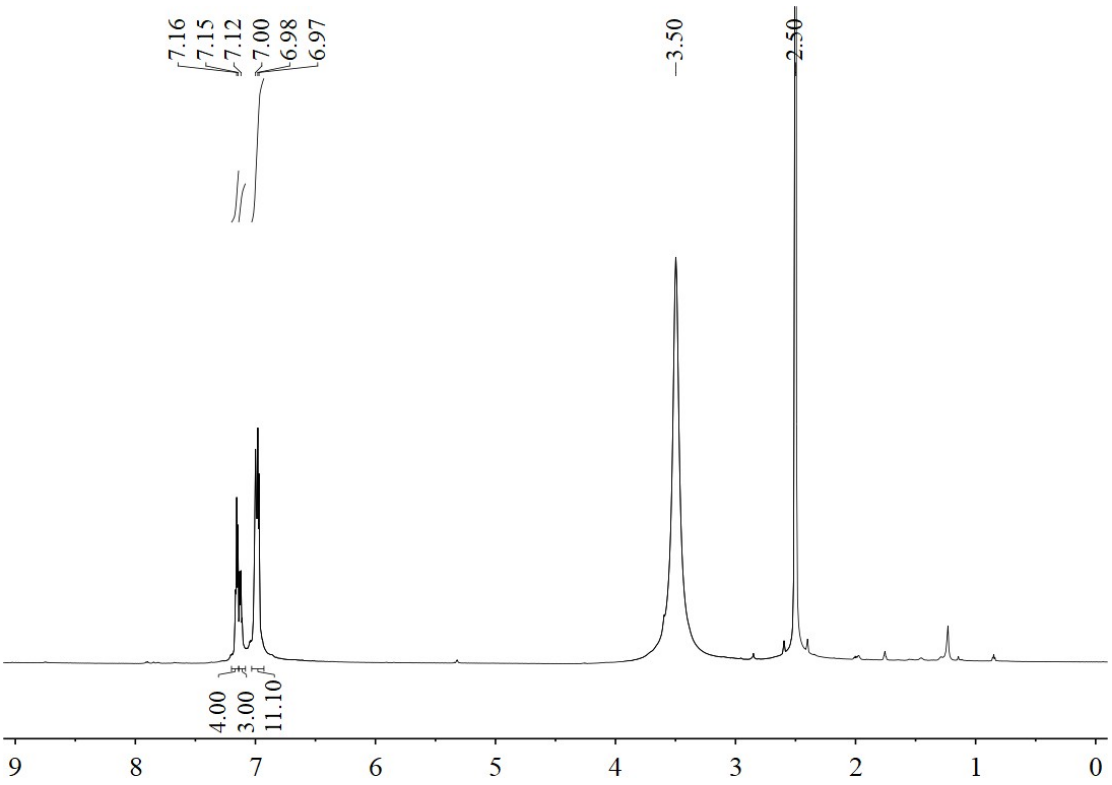

Fig. S11 ^{1}H NMR spectrum of TPE-2NH_3·2NH_2SO_3.

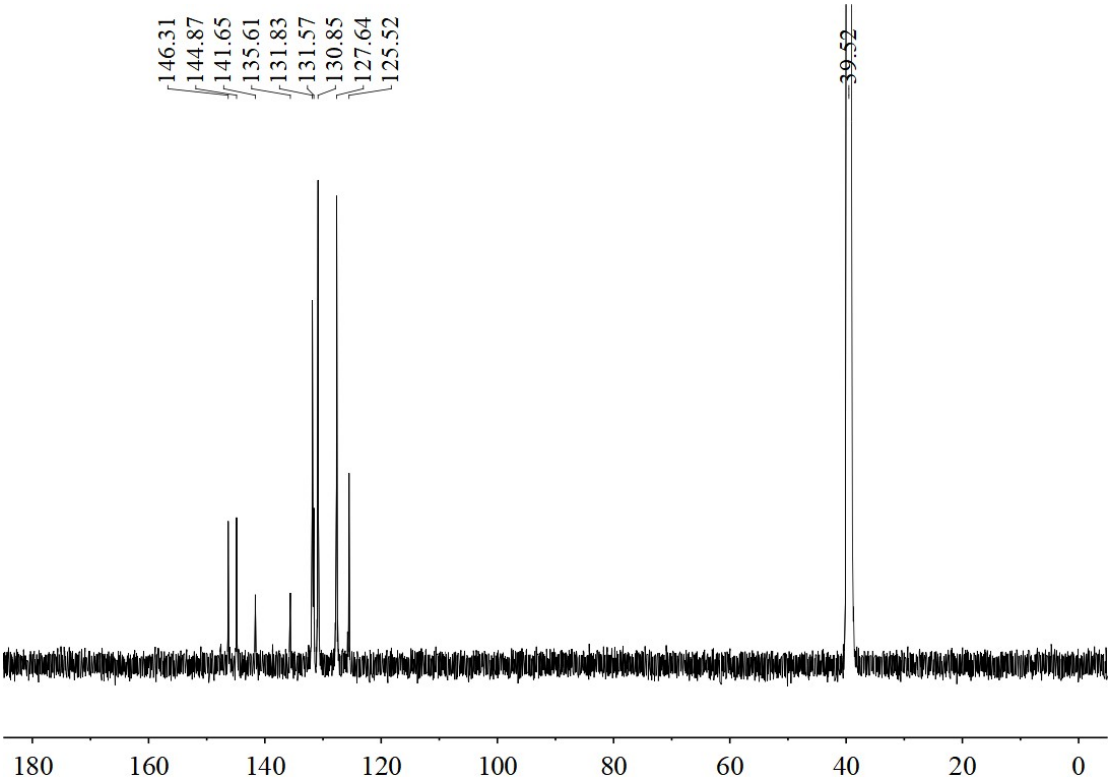

Fig. S12 ^{13}C NMR spectrum of TPE-2NH_3·2NH_2SO_3.

2. UV-Vis absorption spectra

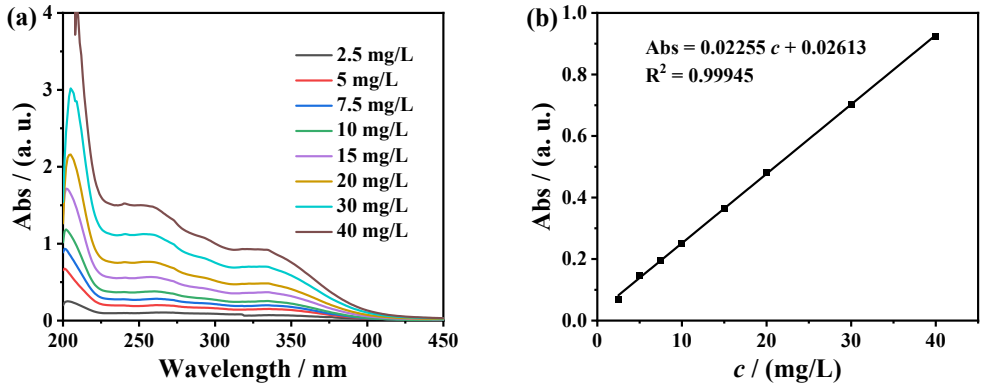

Fig. S13 (a) UV-Vis absorption spectra of the solutions of TPE-2NH_3·SO_4 with various concentrations in ethanol. **(b)** Variation of absorption intensity at 330 nm against concentration.

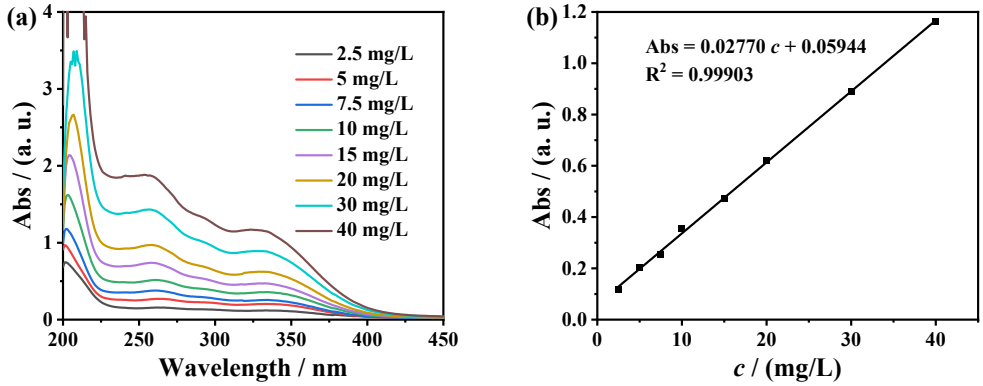

Fig. S14 (a) UV-Vis absorption spectra of the solutions of TPE-2NH_3·2Cl with various concentrations in ethanol. **(b)** Variation of absorption intensity at 330 nm against concentration.

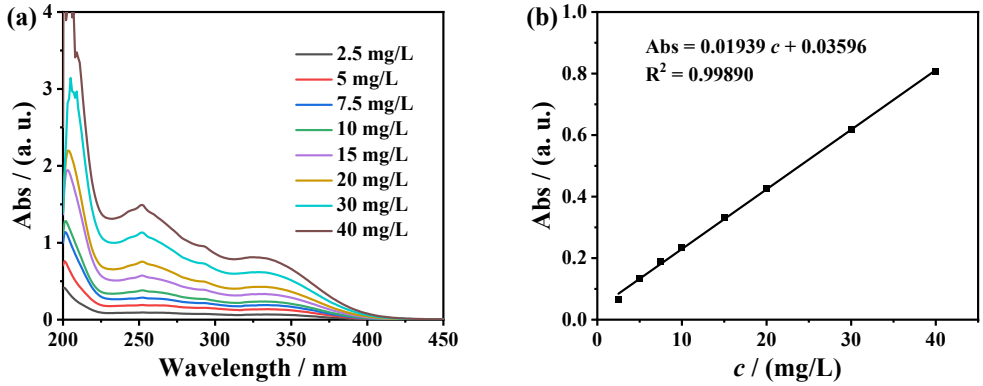

Fig. S15 (a) UV-Vis absorption spectra of the solutions of TPE-2NH_3·2Br with various concentrations in ethanol. (b) Variation of absorption intensity at 330 nm against concentration.

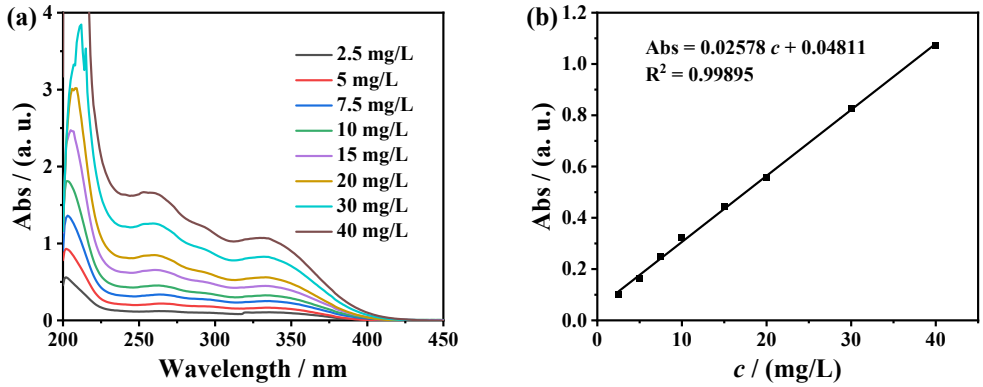

Fig. S16 (a) UV-Vis absorption spectra of the solutions of TPE-2NH_3·2NO_3 with various concentrations in ethanol. (b) Variation of absorption intensity at 330 nm against concentration.

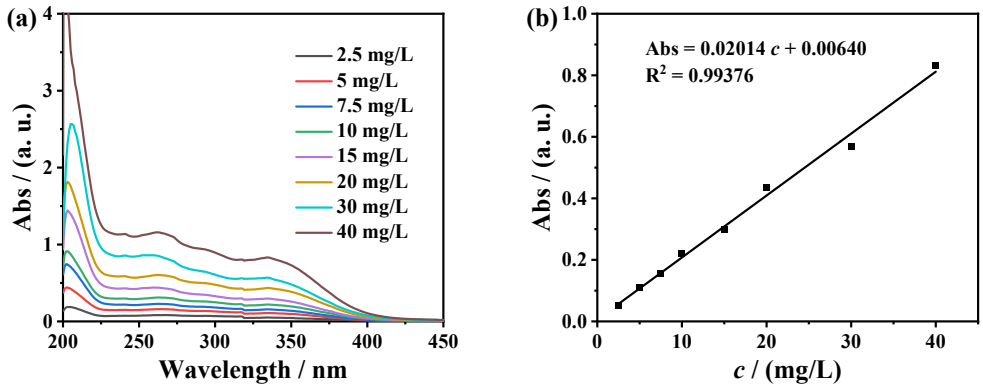

Fig. S17 (a) UV-Vis absorption spectra of the solutions of TPE-2NH_3·2NH_2SO_3 with various concentrations in ethanol. (b) Variation of absorption intensity at 334 nm against concentration.

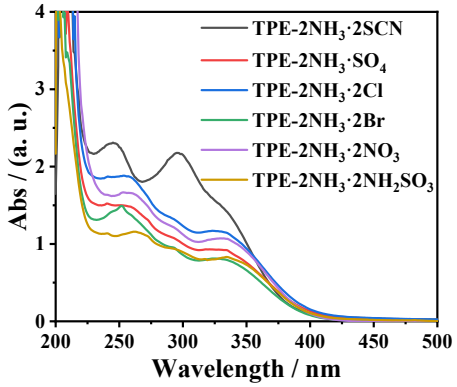

Fig. S18 UV-Vis absorption spectra of the solutions of 40 mg/L TPE-based dicationic compounds in ethanol.

3. AIE characteristic study

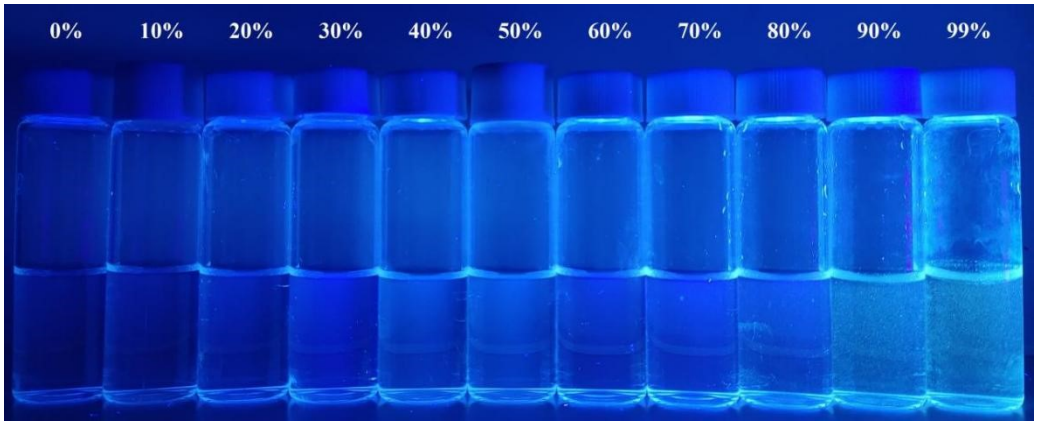

Fig. S19 Photograph of TPE-2$NH_3 \cdot SO_4$ in ethanol/water mixtures with increasing water volume fractions (f_{water}) under 365 nm UV light excitation. Concentration: 40 mg/L.

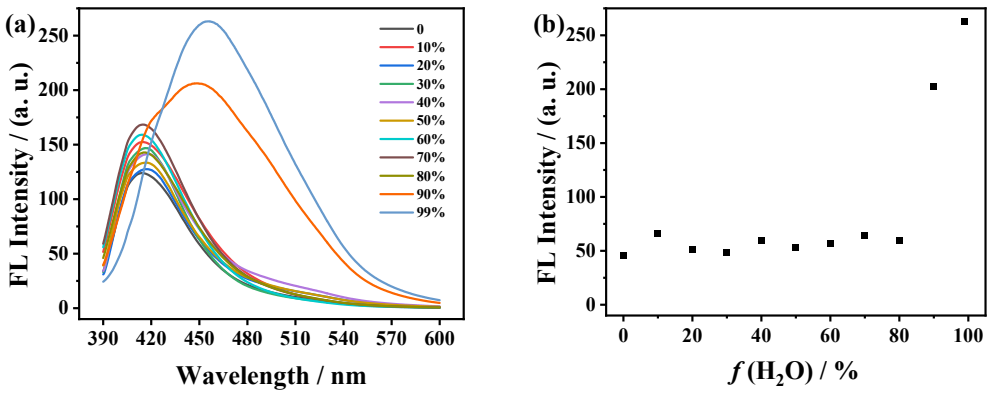

Fig. S20 (a) Emission spectra of TPE-2$NH_3 \cdot SO_4$ in ethanol/water mixtures with 365 nm UV light excitation. Concentration: 40 mg/L. (b) Variation of fluorescence intensity at 457 nm against f_{water}.

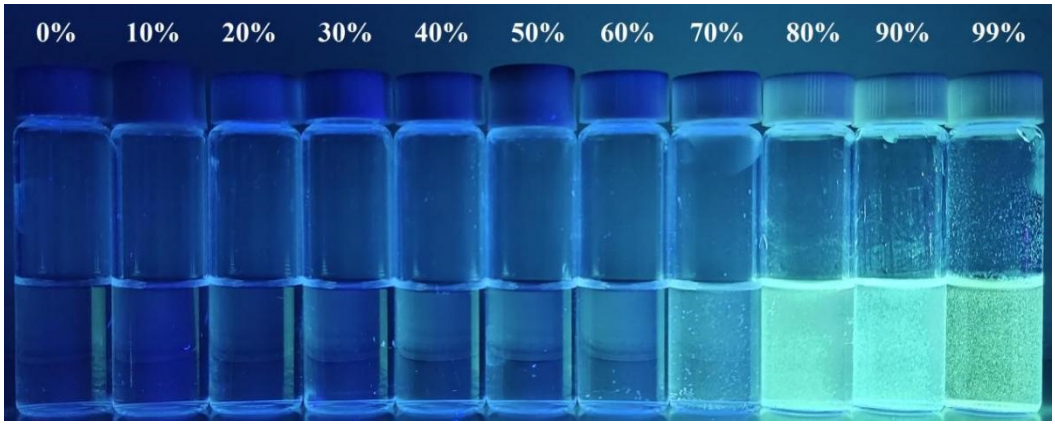

Fig. S21 Photograph of TPE-2$NH_3 \cdot 2Cl$ in ethanol/water mixtures with increasing water volume fractions (f_{water}) under 365 nm UV light excitation. Concentration: 40 mg/L.

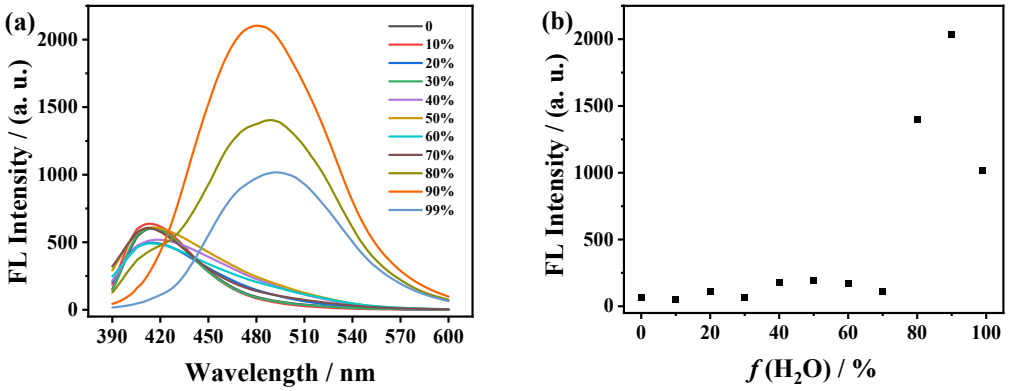

Fig. S22 (a) Emission spectra of TPE-2NH_3·2Cl in ethanol/water mixtures with 365 nm UV light excitation. Concentration: 40 mg/L. (b) Variation of fluorescence intensity at 492 nm against f_{water}.

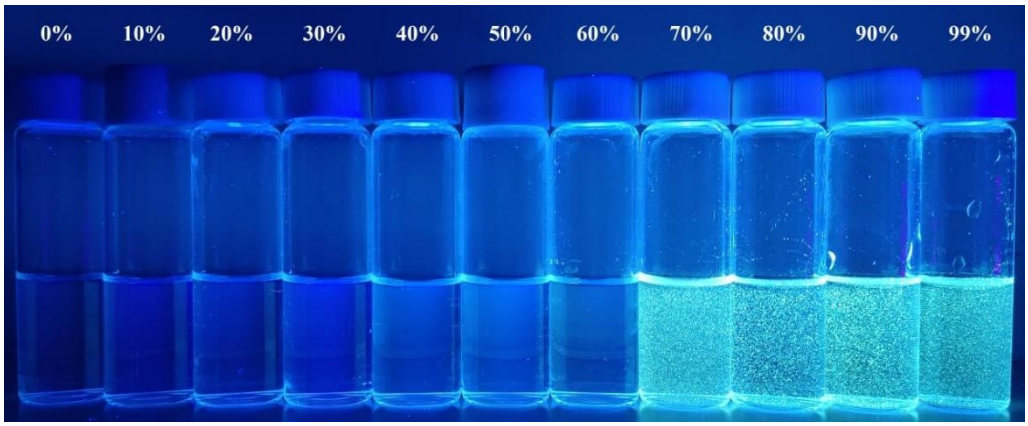

Fig. S23 Photograph of TPE-2NH_3·2Br in ethanol/water mixtures with increasing water volume fractions (f_{water}) under 365 nm UV light excitation. Concentration: 40 mg/L.

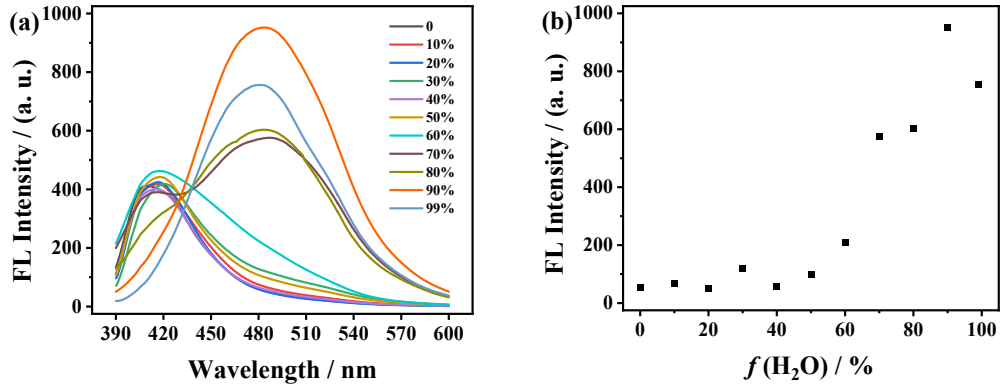

Fig. S24 (a) Emission spectra of TPE-2NH_3·2Br in ethanol/water mixtures with 365 nm UV light excitation. Concentration: 40 mg/L. (b) Variation of fluorescence intensity at 484 nm against f_{water}.

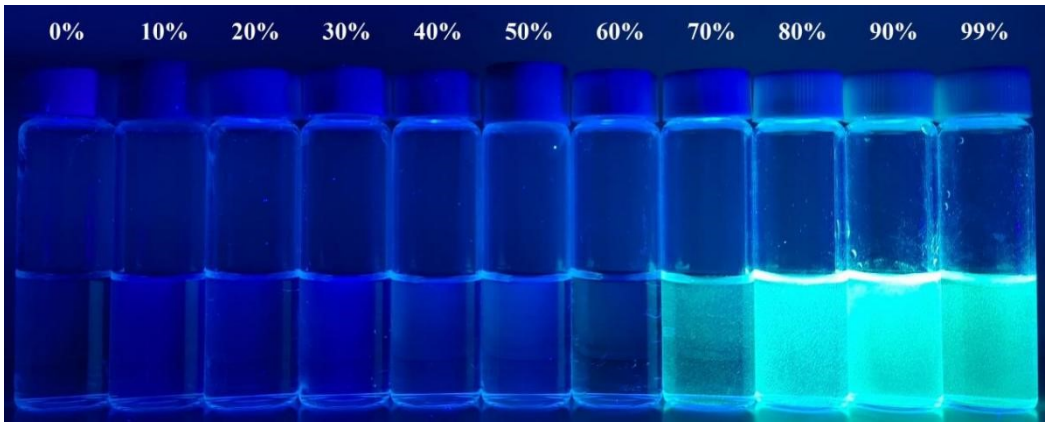

Fig. S25 Photograph of TPE-2NH_3·2NO_3 in ethanol/water mixtures with increasing water volume fractions (f_{water}) under 365 nm UV light excitation. Concentration: 40 mg/L.

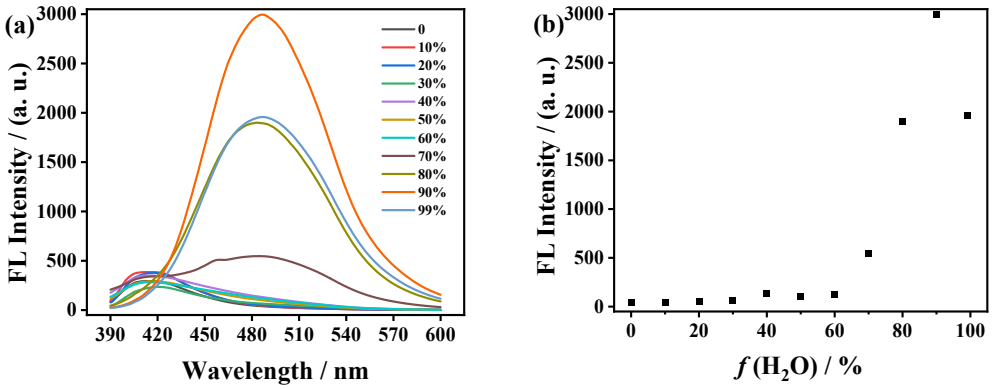

Fig. S26 (a) Emission spectra of TPE-2NH_3·2NO_3 in ethanol/water mixtures with 365 nm UV light excitation. Concentration: 40 mg/L. (b) Variation of fluorescence intensity at 486 nm against f_{water}.

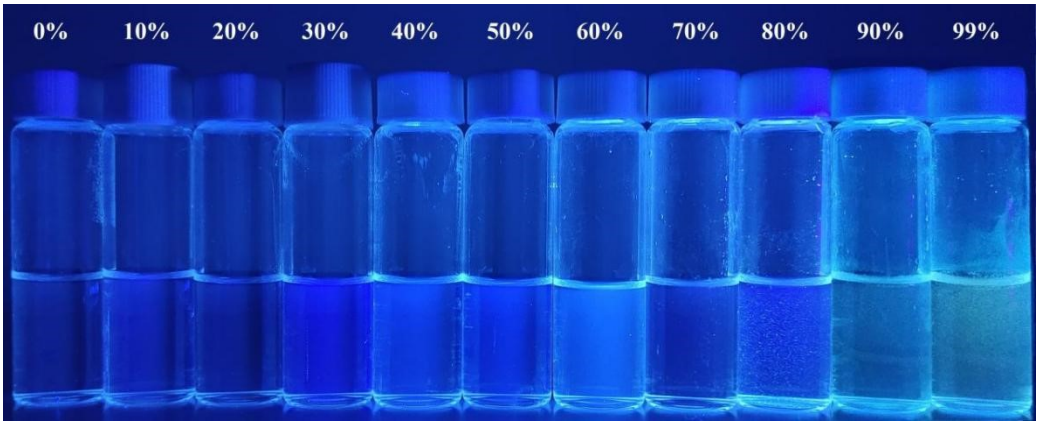

Fig. S27 Photograph of TPE-2NH_3·2NH_2SO_3 in ethanol/water mixtures with increasing water volume fractions (f_{water}) under 365 nm UV light excitation. Concentration: 40 mg/L.

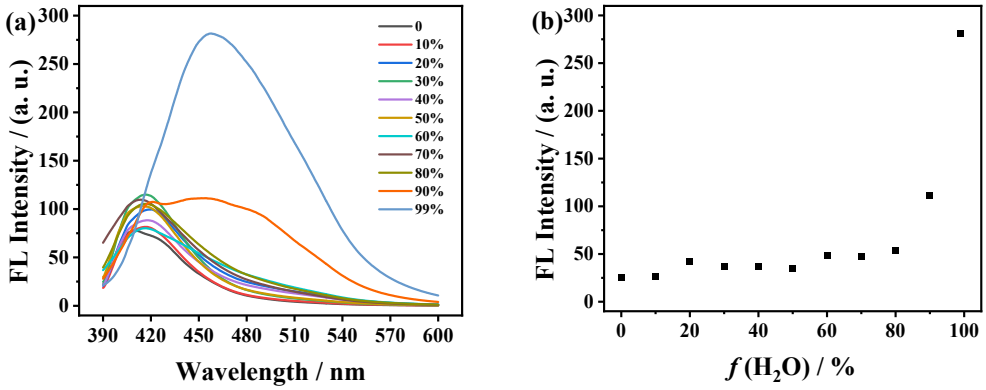

Fig. S28 (a) Emission spectra of TPE-2NH_3·2NH_2SO_3 in ethanol/water mixtures with 365 nm UV light excitation. Concentration: 40 mg/L. (b) Variation of fluorescence intensity at 457 nm against f_{water}.

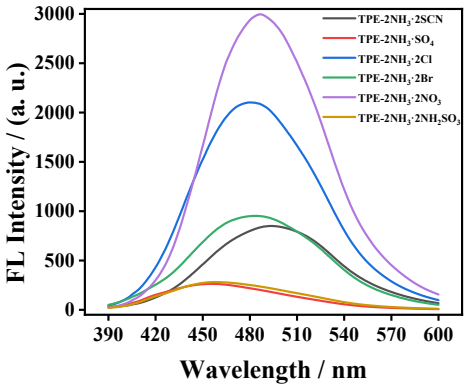

Fig. S29 Emission spectra of 40 mg/L TPE-based dicationic compounds in ethanol/water mixtures with maximum fluorescence intensity under 365 nm UV light excitation.

4. Electrochemical measurements

Figure S30 Equivalent electrical circuit models used to fit EIS data: in 0.5 M H_2SO_4 (left) and in 0.5 M H_2SO_4 in presence of TPE-based compounds (right).

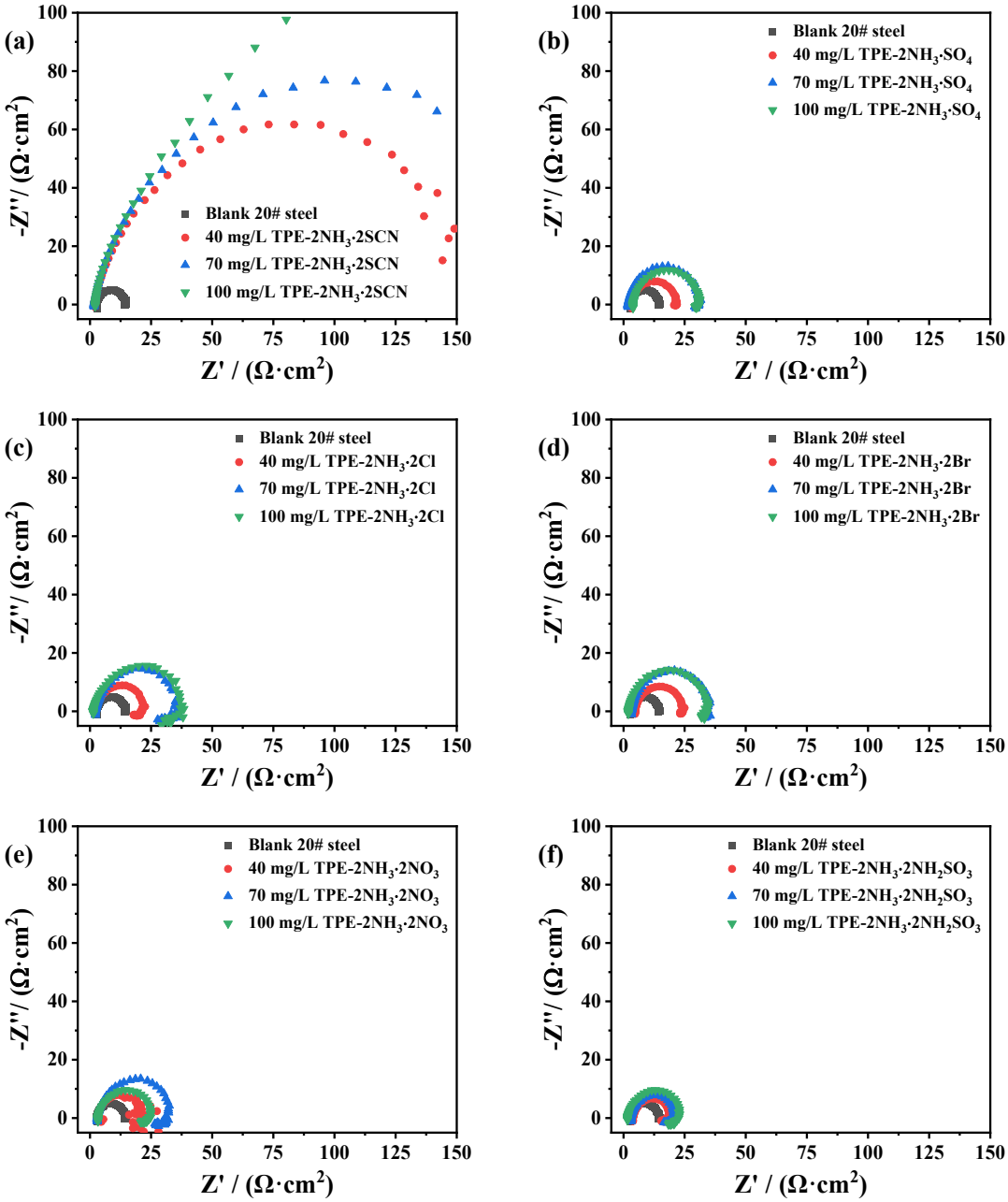

Fig. S31 EIS curves for 20# steel in the absence or presence of various concentrations of (a) TPE-$2NH_3$·2SCN; (b) TPE-$2NH_3$·SO_4; (c) TPE-$2NH_3$·2Cl; (d) TPE-$2NH_3$·2Br; (e) TPE-$2NH_3$·$2NO_3$; (f) TPE-$2NH_3$·$2NH_2SO_3$.

Table S1 Electrochemical parameters of 20# steel in the absence or presence of different concentrations of TPE-based dicationic compounds by EIS measurements in 0.5 M H_2SO_4.

Inhibitor	c / (mg/L)	R_s / (Ω/cm^2)	R_{ct} / (Ω/cm^2)	η_E / %
Blank	—	2.7	11.8	—
TPE-2NH$_3$·2SCN	40	1.6	156.5	92.5
	70	1.5	192.2	93.9
	100	1.9	287.9	95.9
TPE-2NH$_3$·SO$_4$	40	3.3	18.6	36.5
	70	1.9	29.4	59.9
	100	3.8	27.9	57.7
TPE-2NH$_3$·2Cl	40	1.9	20.8	43.4
	70	2.2	35.0	66.3
	100	2.1	35.1	66.4
TPE-2NH$_3$·2Br	40	4.7	19.9	40.8
	70	3.2	32.5	63.7
	100	2.5	34.0	65.3
TPE-2NH$_3$·2NO$_3$	40	3.3	20.5	42.3
	70	2.9	31.1	62.1
	100	3.2	22.7	48.1
TPE-2NH$_3$·2NH$_2$SO$_3$	40	3.9	15.4	23.5
	70	3.0	18.5	36.4
	100	2.7	22.8	48.3

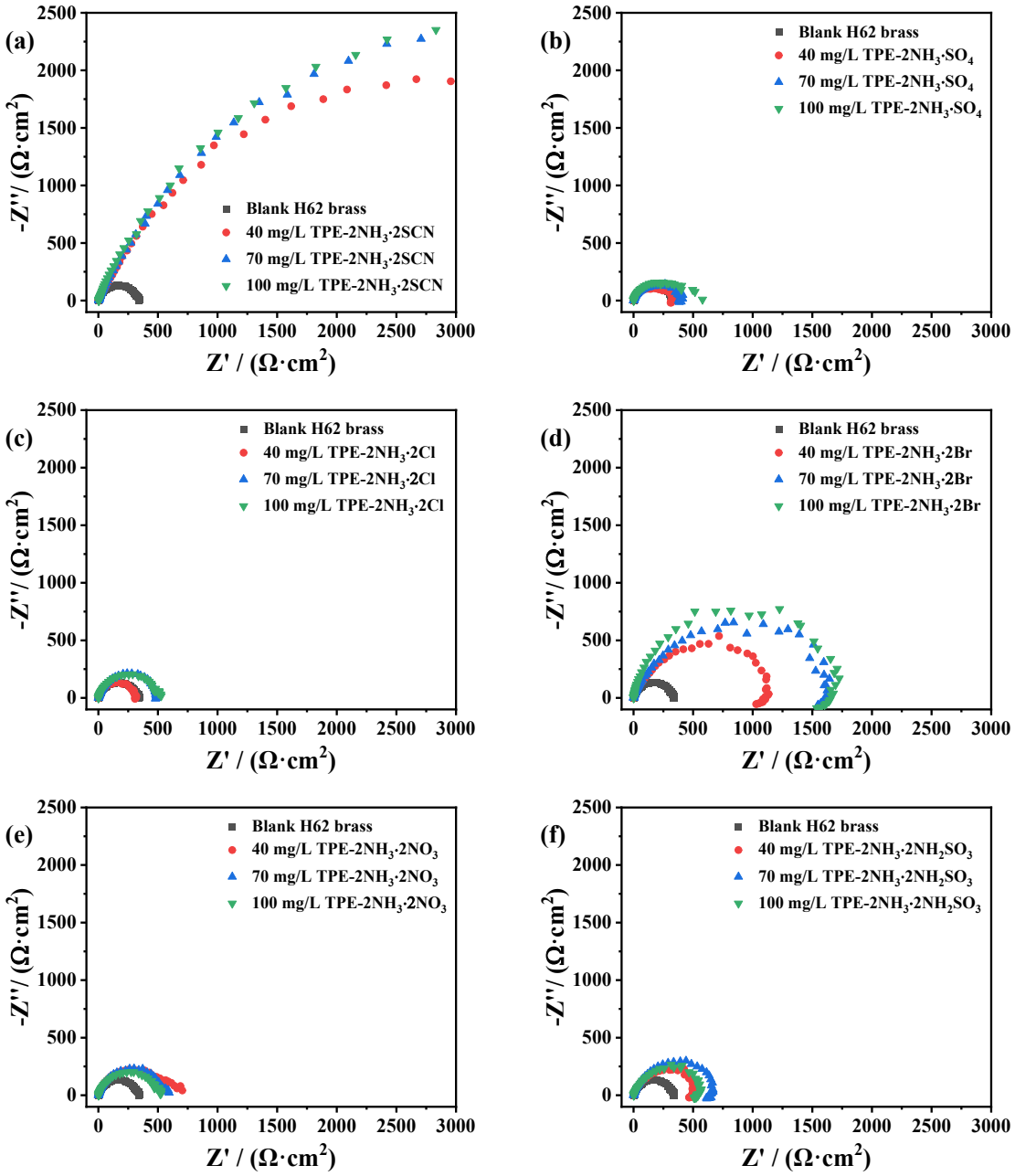

Fig. S32 EIS curves for H62 brass in the absence or presence of various concentrations of (a) TPE-$2NH_3{\cdot}2SCN$; (b) TPE-$2NH_3{\cdot}SO_4$; (c) TPE-$2NH_3{\cdot}2Cl$; (d) TPE-$2NH_3{\cdot}2Br$; (e) TPE-$2NH_3{\cdot}2NO_3$; (f) TPE-$2NH_3{\cdot}2NH_2SO_3$.

Table S2 Electrochemical parameters of H62 brass in the absence or presence of different concentrations of TPE-based dicationic compounds by EIS measurements in 0.5 M H_2SO_4.

Inhibitor	c / (mg/L)	R_s / (Ω/cm^2)	R_{ct} / (Ω/cm^2)	η_E / %
Blank	—	2.0	331.2	—
TPE-2NH$_3$·2SCN	40	2.1	5492.0	94.0
	70	2.5	6515.0	94.9
	100	2.9	6773.0	95.1
TPE-2NH$_3$·SO$_4$	40	1.1	341.1	2.9
	70	1.6	400.8	17.4
	100	1.3	508.0	34.8
TPE-2NH$_3$·2Cl	40	2.2	312.9	-5.8
	70	1.4	497.8	33.5
	100	1.3	495.2	33.1
TPE-2NH$_3$·2Br	40	2.3	1104.0	70.0
	70	1.8	1610.0	79.4
	100	2.1	1650.8	79.9
TPE-2NH$_3$·2NO$_3$	40	1.8	597.9	44.6
	70	1.5	554.2	40.2
	100	1.5	534.0	38.0
TPE-2NH$_3$·2NH$_2$SO$_3$	40	2.3	502.1	34.0
	70	2.3	659.8	49.8
	100	2.3	559.7	40.8

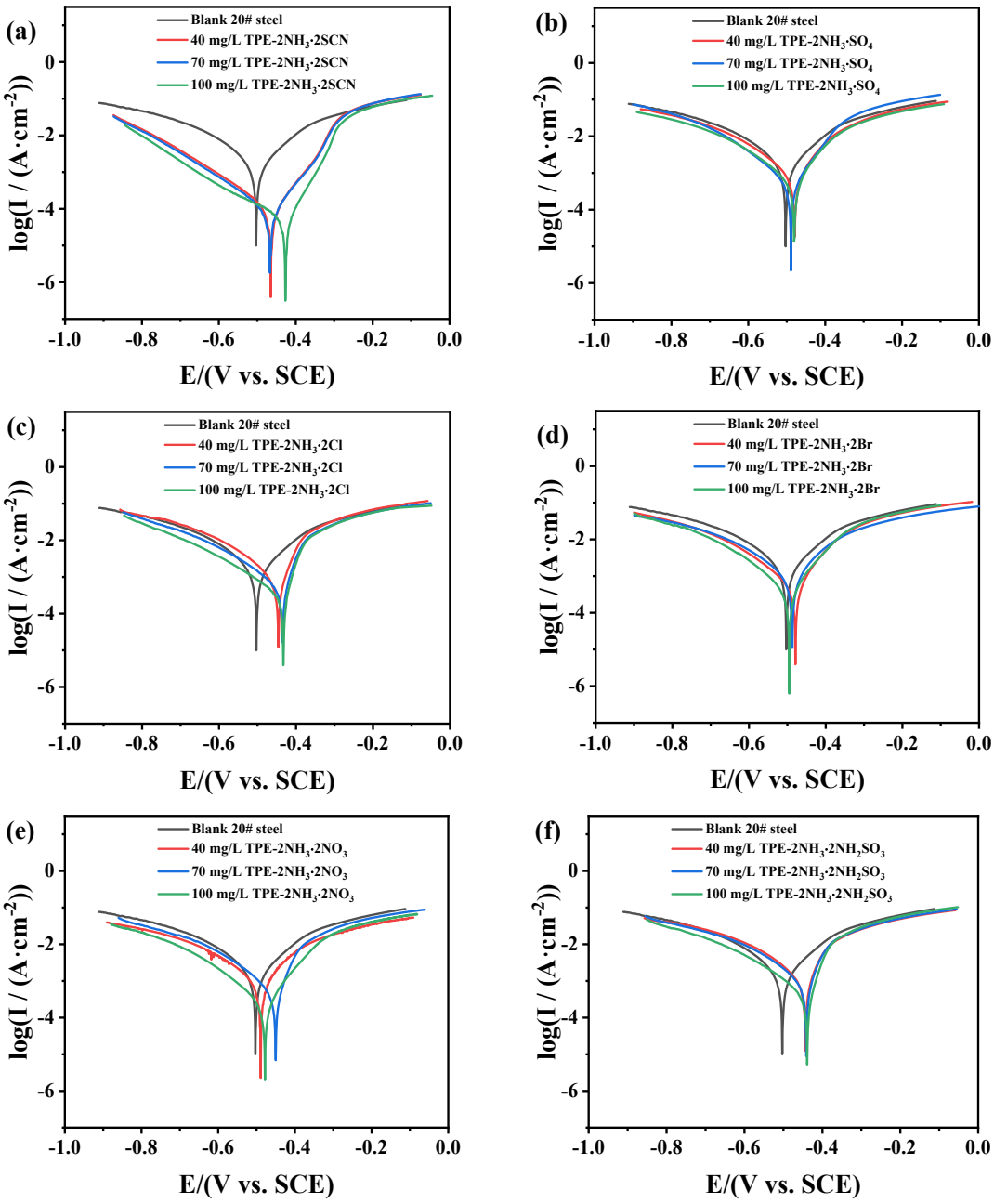

Fig. S33 PDP curves for 20# steel in the absence or presence of various concentrations of (a) TPE-$2NH_3$·2SCN; (b) TPE-$2NH_3$·SO_4; (c) TPE-$2NH_3$·2Cl; (d) TPE-$2NH_3$·2Br; (e) TPE-$2NH_3$·$2NO_3$; (f) TPE-$2NH_3$·$2NH_2SO_3$.

Table S3 Electrochemical parameters of 20# steel in the absence or presence of different concentrations of TPE-based dicationic compounds by potentiodynamic polarization measurements in 0.5 M H_2SO_4.

Inhibitor	*c*/(mg/L)	I_{corr}/(μA/cm^2)	E_{corr}/V	β_c/(mV/dec)	β_a/(mV/dec)	η_p/%
Blank	—	1701.0	-0.503	146.3	113.2	—
TPE-2NH$_3$·2SCN	40	97.3	-0.465	139.3	77.2	94.3
	70	97.3	-0.467	140.5	80.4	94.3
	100	55.1	-0.427	203.2	51.5	96.8
TPE-2NH$_3$·SO$_4$	40	1046.0	-0.479	136.6	109.2	38.5
	70	621.9	-0.489	126.1	71.9	63.4
	100	718.0	-0.481	136.0	100.8	57.8
TPE-2NH$_3$·2Cl	40	1331.0	-0.446	135.2	154.9	21.8
	70	1155.0	-0.435	142.0	170.4	32.1
	100	786.1	-0.433	149.3	163.3	53.8
TPE-2NH$_3$·2Br	40	1096.0	-0.487	144.2	123.0	35.6
	70	631.5	-0.479	131.1	96.5	62.9
	100	489.3	-0.495	124.3	88.6	71.2
TPE-2NH$_3$·2NO$_3$	40	1143.1	-0.489	155.4	127.6	32.8
	70	844.7	-0.45	132.9	145.6	50.3
	100	589.0	-0.478	166.8	139.6	65.4
TPE-2NH$_3$·2NH$_2$SO$_3$	40	1794.0	-0.444	142.3	167.1	-5.5
	70	1757.0	-0.441	141.2	182.2	-3.3
	100	827.6	-0.439	142.3	155.0	51.3

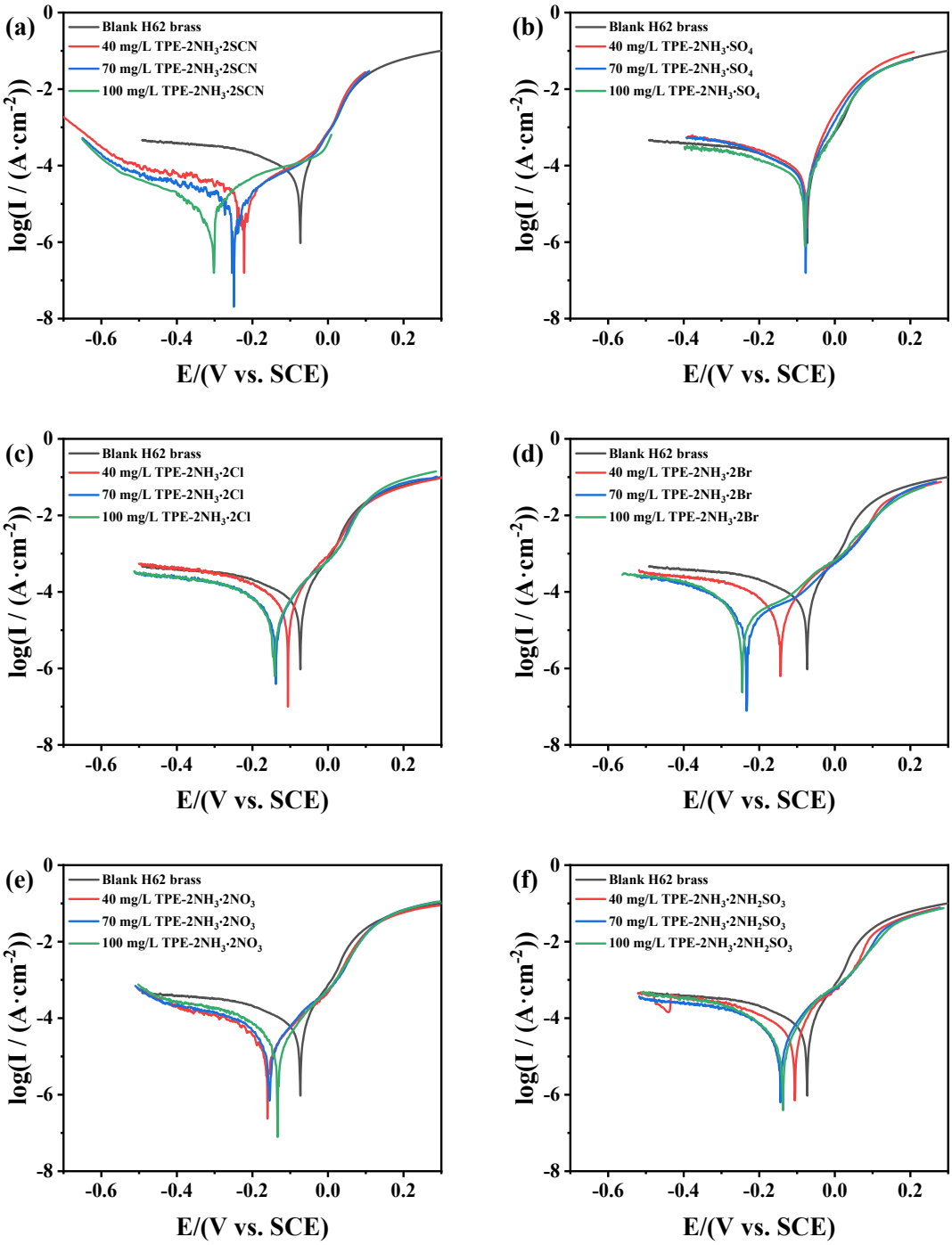

Fig. S34 PDP curves for H62 brass in the absence or presence of various concentrations of (a) TPE-$2NH_3$·2SCN; (b) TPE-$2NH_3$·SO_4; (c) TPE-$2NH_3$·2Cl; (d) TPE-$2NH_3$·2Br; (e) TPE-$2NH_3$·$2NO_3$; (f) TPE-$2NH_3$·$2NH_2SO_3$.

Table S4 Electrochemical parameters of H62 brass in the absence or presence of different concentrations of TPE-based dicationic compounds by potentiodynamic polarization measurements in 0.5 M H_2SO_4.

Inhibitor	c/(mg/L)	I_{corr}/(μA/cm^2)	E_{corr}/V	β_c/(mV/dec)	β_a/(mV/dec)	η_P/%
Blank	—	84.7	-0.073	227.0	55.0	—
TPE-2NH$_3$·2SCN	40	22.8	-0.222	366.3	180.6	73.1
	70	10.9	-0.249	246.1	164.8	87.1
	100	7.1	-0.302	147.1	180.0	91.7
TPE-2NH$_3$·SO$_4$	40	90.3	-0.074	224.6	68.4	-6.6
	70	67.7	-0.077	211.1	59.3	20.1
	100	44.7	-0.079	264.9	54.3	47.2
TPE-2NH$_3$·2Cl	40	62.2	-0.106	206.7	92.3	26.5
	70	36.5	-0.138	193.8	105.0	57.0
	100	31.0	-0.141	205.1	109.0	63.5
TPE-2NH$_3$·2Br	40	35.5	-0.234	186.9	232.8	58.1
	70	27.3	-0.187	159.8	95.7	67.8
	100	36.4	-0.245	177.5	213.1	57.0
TPE-2NH$_3$·2NO$_3$	40	42.0	-0.16	214.3	102.0	50.4
	70	39.0	-0.155	266.1	99.3	54.0
	100	31.3	-0.133	184.6	94.6	63.0
TPE-2NH$_3$·2NH$_2$SO$_3$	40	77.9	-0.106	210.7	143.4	8.1
	70	41.6	-0.144	210.3	114.7	50.9
	100	32.6	-0.137	165.7	104.1	61.5

5. SEM images

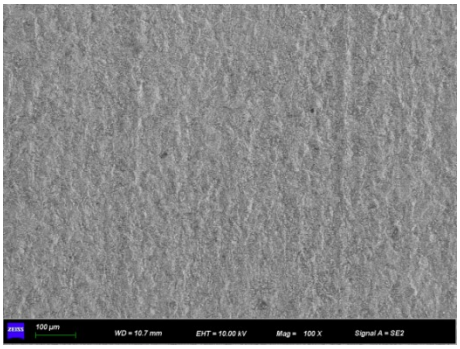

(a)

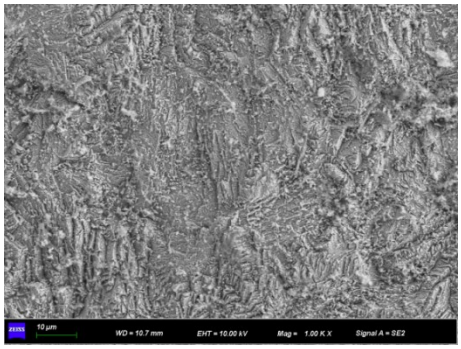

(b)

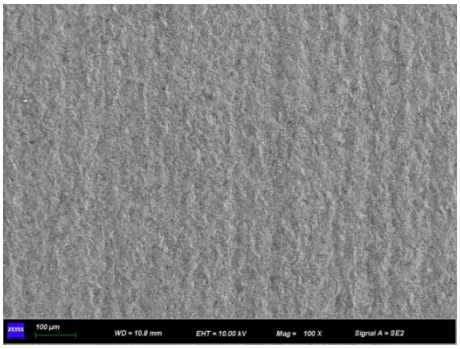

(c)

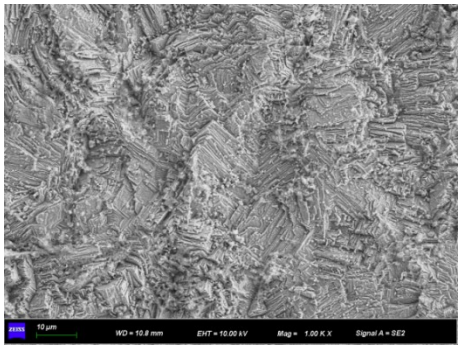

(d)

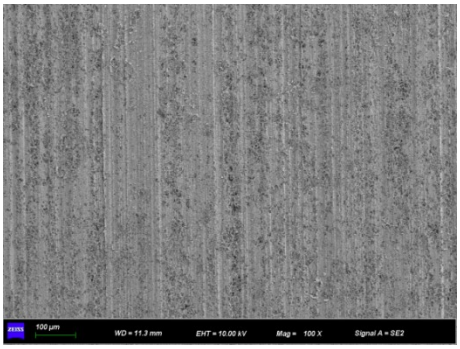

(e)

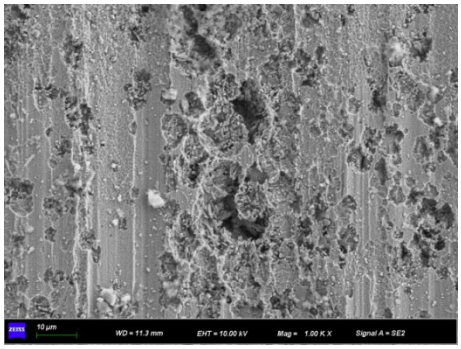

(f)

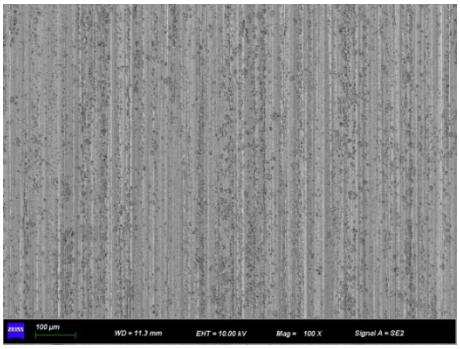

(g)

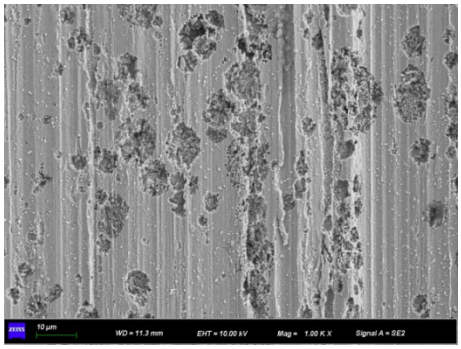

(h)

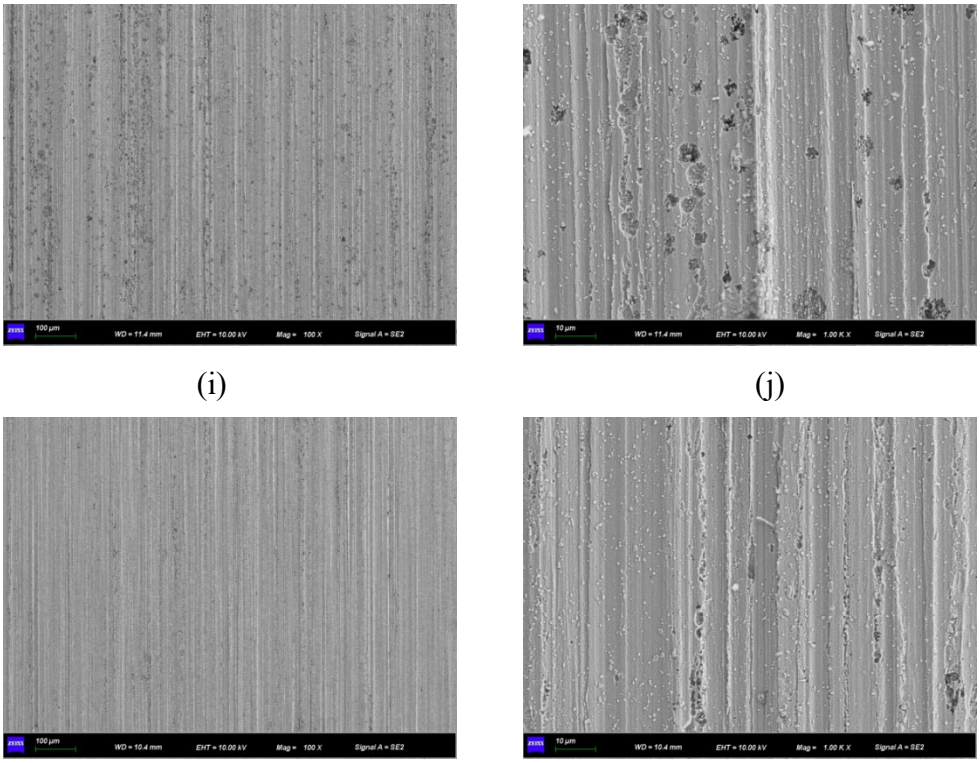

Fig. S35 SEM images of 20# steel coupons in the presence of different concentrations of TPE-$2NH_3 \cdot 2SCN$ after weight loss experiment: (a, b) 5 mg/L; (c, d) 10 mg/L; (e, f) 20 mg/L; (g, h) 40 mg/L; (i, j) 70 mg/L; (k, l) 200 mg/L. Scale: 100 μm for (a, c, e, g, i, k) and 10 μm for (b, d, f, h, j, l).

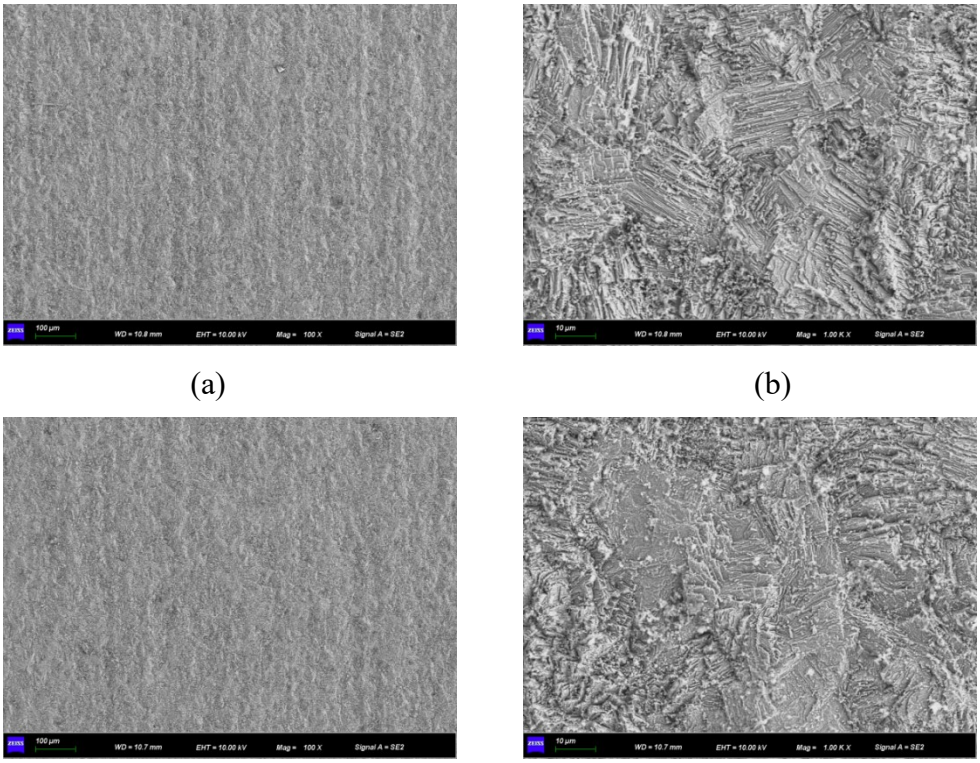

Fig. S36 SEM images of 20# steel coupons in the presence of different concentrations of TPE-$2NH_3 \cdot SO_4$ after weight loss experiment: (a, b) 40 mg/L; (c, d) 70 mg/L. Scale: 100 μm for (a, c) and 10 μm for (b, d).

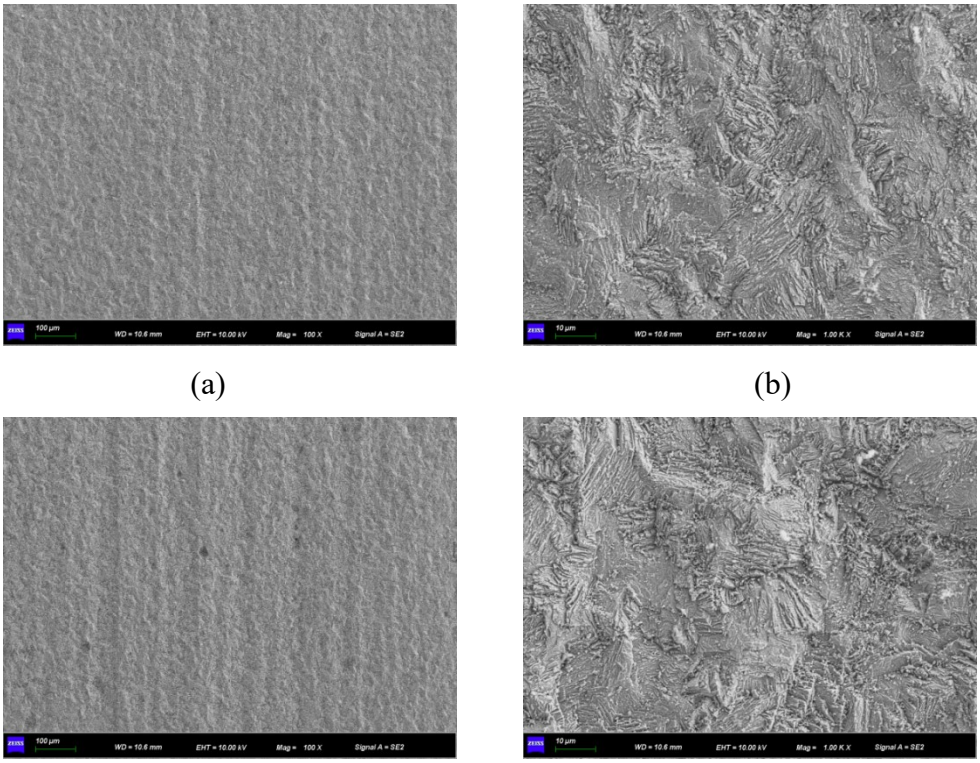

Fig. S37 SEM images of 20# steel coupons in the presence of different concentrations of TPE-$2NH_3 \cdot 2Cl$ after weight loss experiment: (a, b) 40 mg/L; (c, d) 70 mg/L. Scale: 100 μm for (a, c) and 10 μm for (b, d).

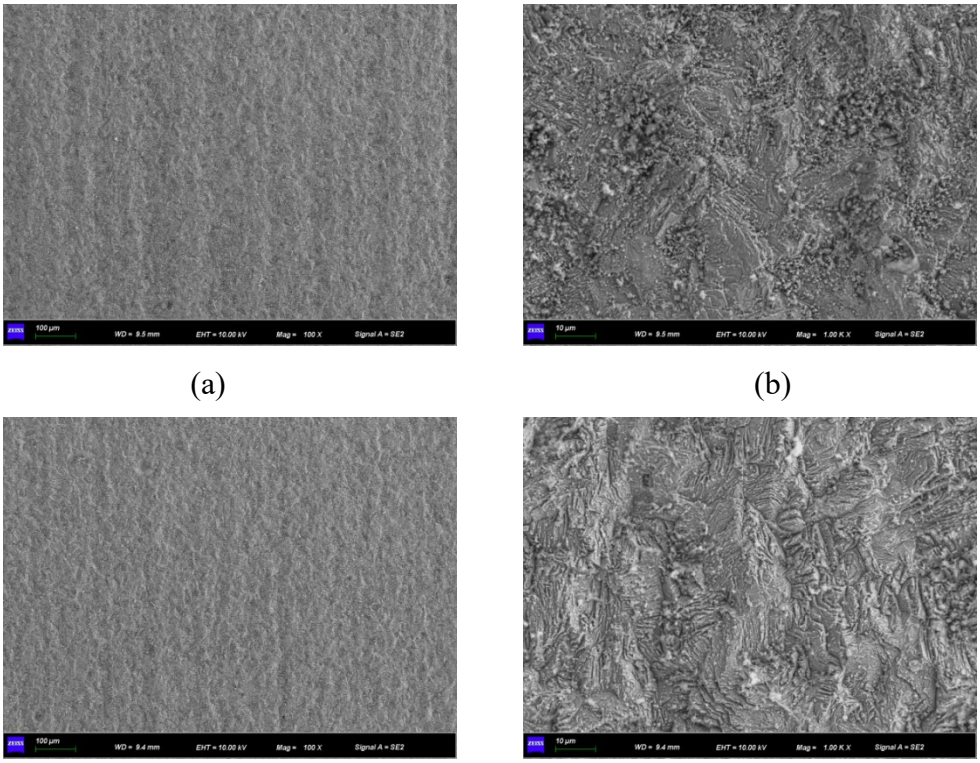

Fig. S38 SEM images of 20# steel coupons in the presence of different concentrations of TPE-2NH_3·2Br after weight loss experiment: (a, b) 40 mg/L; (c, d) 70 mg/L. Scale: 100 μm for (a, c) and 10 μm for (b, d).

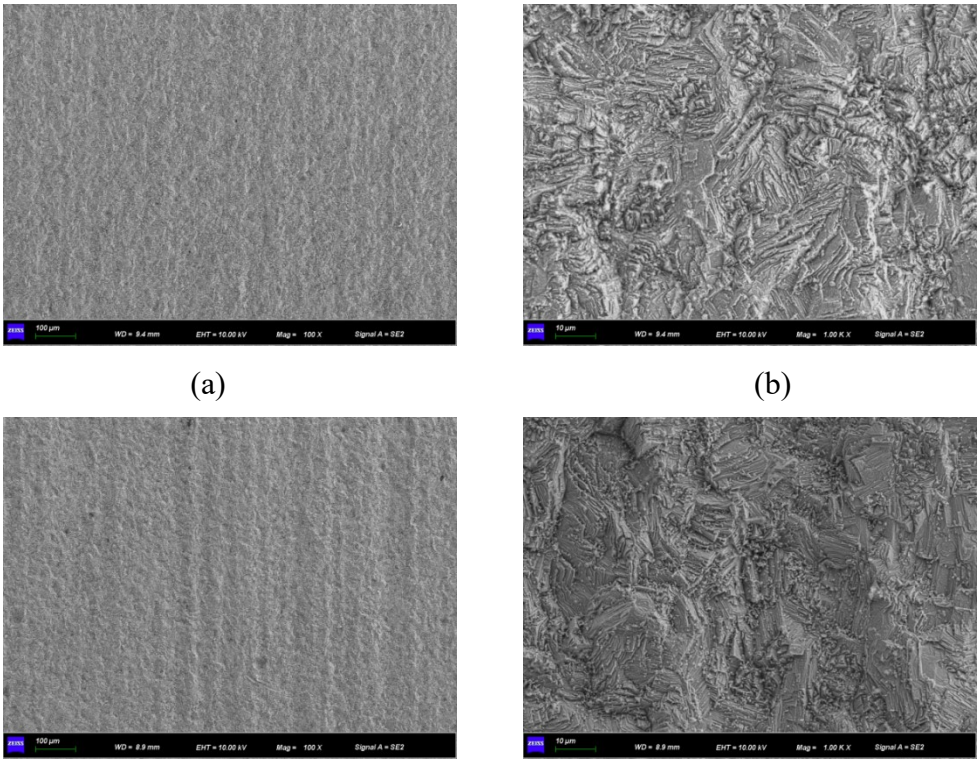

Fig. S39 SEM images of 20# steel coupons in the presence of different concentrations of TPE-$2NH_3 \cdot 2NO_3$ after weight loss experiment: (a, b) 40 mg/L; (c, d) 70 mg/L. Scale: 100 μm for (a, c) and 10 μm for (b, d).

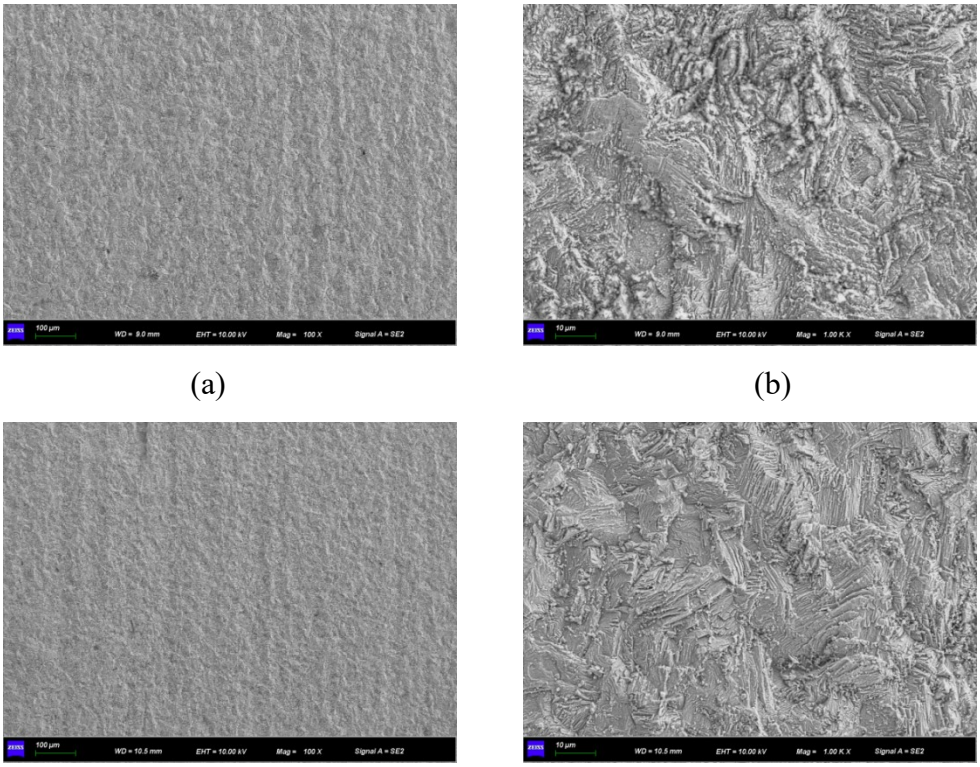

Fig. S40 SEM images of 20# steel coupons in the presence of different concentration of TPE-$2NH_3 \cdot 2NH_2SO_3$ after weight loss experiment: (a, b) 40 mg/L; (c, d) 70 mg/L. Scale: 100 μm for (a, c) and 10 μm for (b, d).

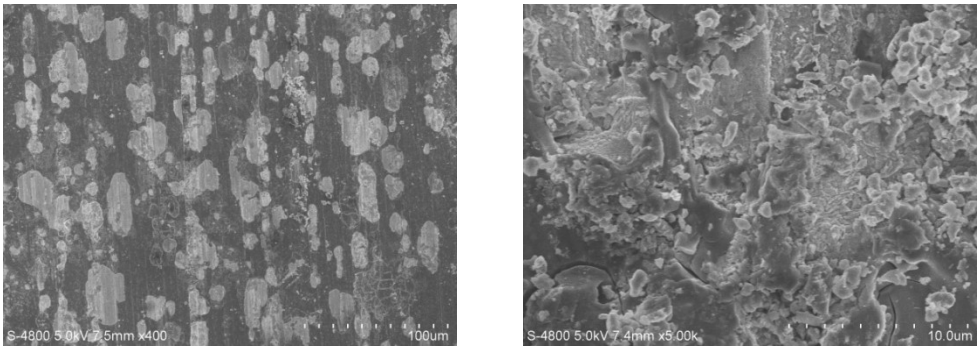

(a) (b)

Fig. S41 SEM images of H62 coupon in the presence of 70 mg/L TPE-2NH_3·2SCN after weight loss experiment. Scale: (a) 100 μm; (b) 10 μm.

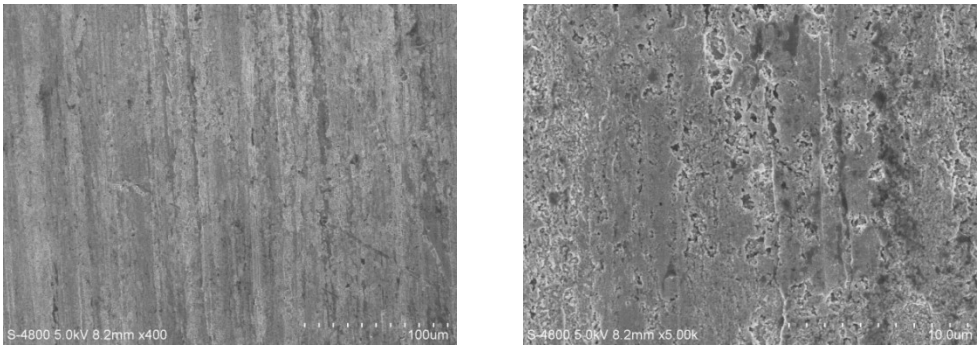

(a) (b)

Fig. S42 SEM images of H62 coupon in the presence of 70 mg/L TPE-2NH_3·SO_4 after weight loss experiment. Scale: (a) 100 μm; (b) 10 μm.

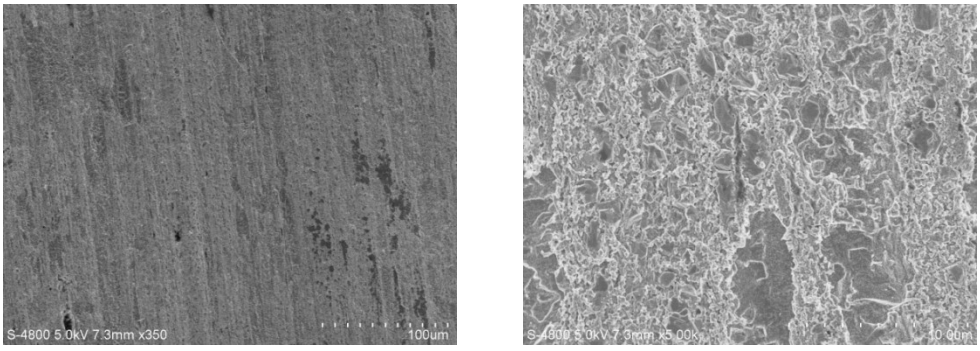

(a) (b)

Fig. S43 SEM images of H62 coupon in the presence of 70 mg/L TPE-2NH_3·2Cl after weight loss experiment. Scale: (a) 100 μm; (b) 10 μm.

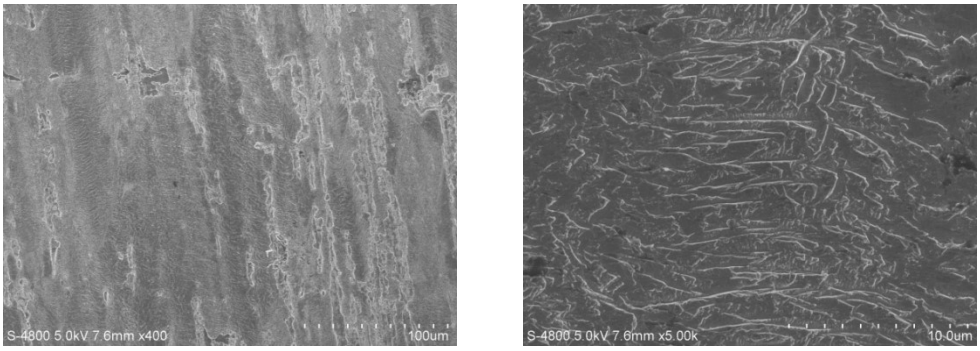

(a) (b)

Fig. S44 SEM images of H62 coupon in the presence of 70 mg/L TPE-2NH_3·2Br after weight loss experiment. Scale: (a) 100 μm; (b) 10 μm.

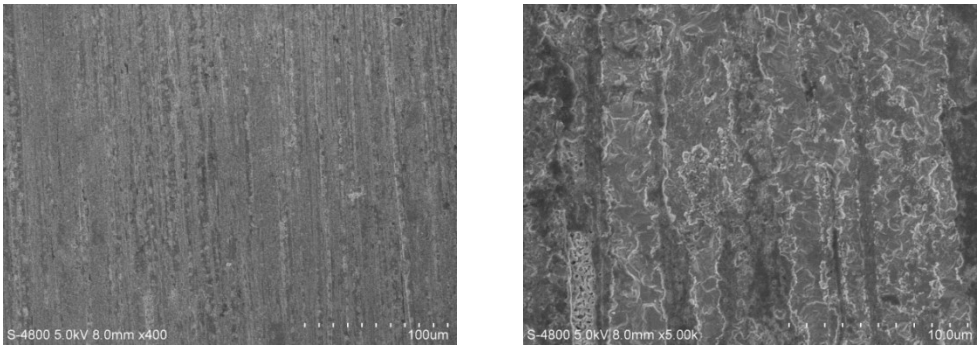

(a) (b)

Fig. S45 SEM images of H62 coupon in the presence of 70 mg/L TPE-2NH_3·2NO_3 after weight loss experiment. Scale: (a) 100 μm; (b) 10 μm.

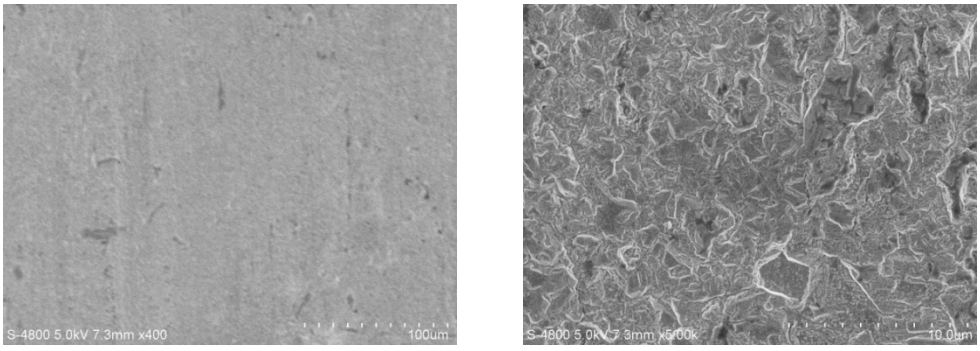

Fig. S46 SEM images of H62 coupon in the presence of 70 mg/L TPE-2NH_3·2NH_2SO_3 after weight loss experiment. Scale: (a) 100 μm; (b) 10 μm.

6. XPS data

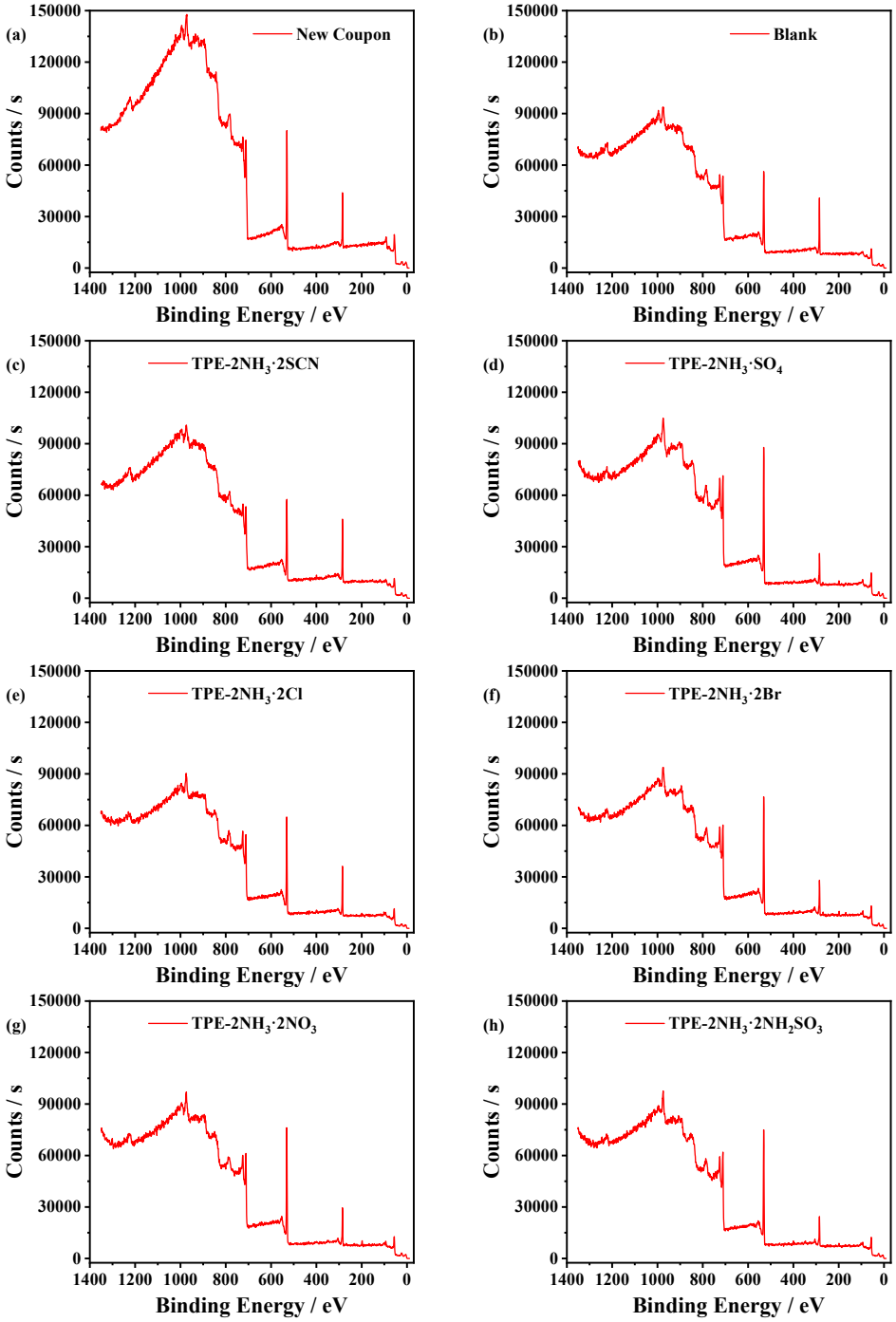

Fig. S47 The XPS full spectra of 20# steel coupons: (a) new coupon before corrosion; (b) blank sample after weight loss experiment; in the presence of 100 mg/L (c) TPE-2NH_3·2SCN, (d) TPE-2NH_3·SO_4, (e) TPE-2NH_3·2Cl, (f) TPE-2NH_3·2Br, (g) TPE-2NH_3·2NO_3, (h) TPE-2NH_3·2NH_2SO_3 after weight loss experiment.

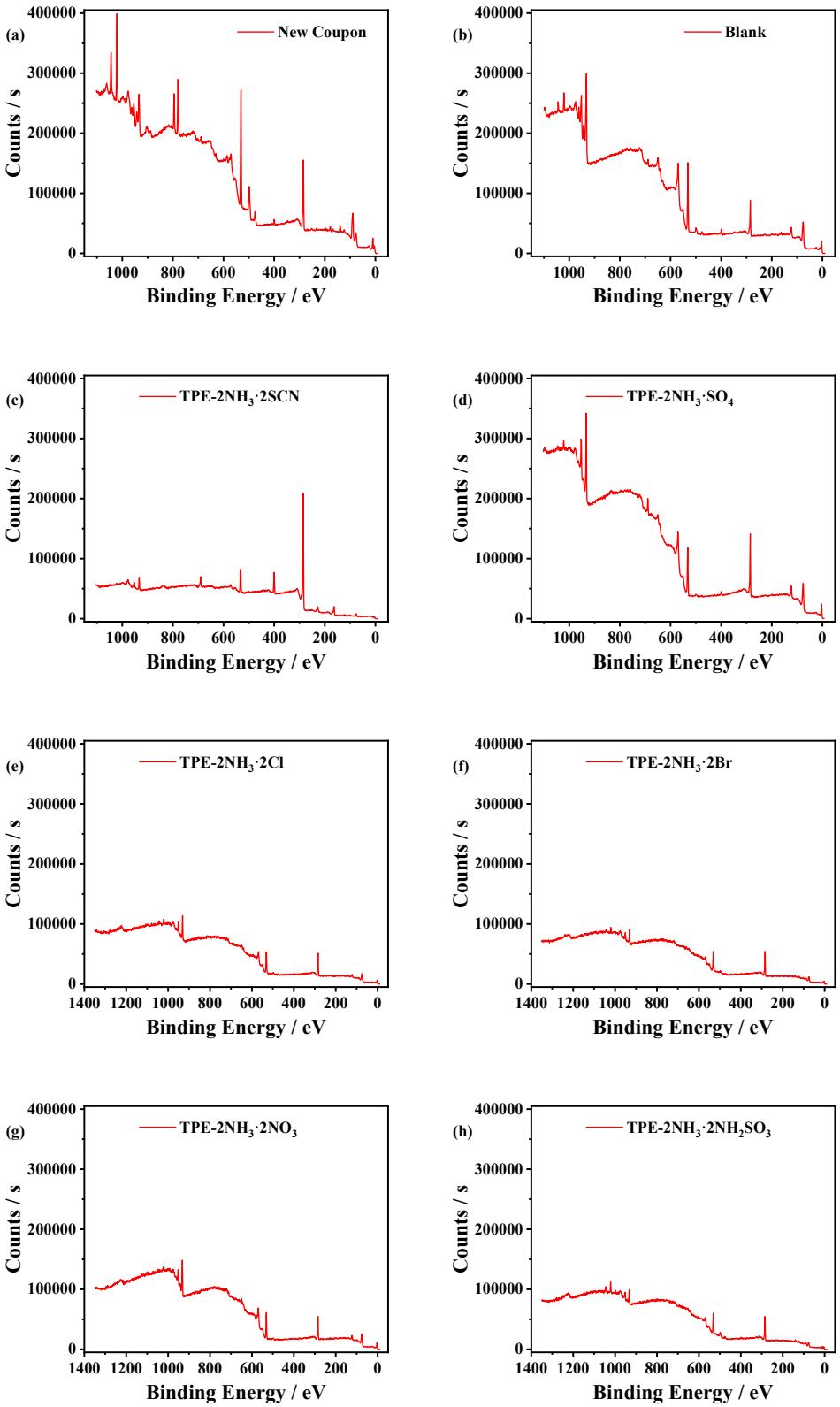

Fig. S48 The XPS full spectra of H62 brass coupons: (a) new coupon before corrosion; (b) blank sample after weight loss experiment; in the presence of 100 mg/L (c) TPE-2NH_3·2SCN, (d) TPE-2NH_3·SO_4, (e) TPE-2NH_3·2Cl, (f) TPE-2NH_3·2Br, (g) TPE-2NH_3·2NO_3, (h) TPE-2NH_3·2NH_2SO_3 after weight loss experiment.

7. Corrosion inhibitors in literature

Table S5 List of corrosion inhibitors for carbon steel in literature.

Inhibitor	Concentration	Carbon steel	Acid solution	Method	Temperature	Inhibition efficiency	Mechanism of action	ΔG_{ads} (kJ/mol)	Adsorption isotherm	Reference
Dodecyl trimethyl ammonium bromide (DTAB)-Thiourea	10^{-3}M	Q235	0.05 M H_2SO_4	Weight-loss	30°C	93.37%				[S6]
Dodecyl dimethyl benzyl ammonium bromide (DDBAB)-Thiourea	10^{-3}M	Q235	0.05 M H_2SO_4	Weight-loss	30°C	94.98%				[S6]
Trans-cinnamaldehyde	1000 ppm	IS2062 mild steel	1 M HCl	Weight-loss	27°C	91%	Mixed-type	-23.53	Temkin	[S7]
OMID	0.1 mM	Carbon steel	1 M HCl	Weight-loss	Room temperature	~97%	Mixed-type			[S8]
1-butyl-2,3-dimethylimidazolium iodide $[DBIM]^+I^-$	100 ppm	API 5L X52	1 M H_2SO_4	PDP		95%	Mixed-type	-35.5	Langmuir	[S9]
1-propyl-2,3-dimethylimidazolium iodide $[DPIM]^+I^-$	100 ppm	API 5L X52	1 M H_2SO_4	PDP		96%	Mixed-type	-37.6	Langmuir	[S9]
amino acid zwitterion(Z-1)	300.8 µM	Mild steel	1 M HCl	Weight-loss	303 K	95.40%	Mixed-type	-37.64	Langmuir	[S10]
amino acid zwitterion(Z-2)	15.04 µM	Mild steel	1 M HCl	Weight-loss	303 K	96.22%	Mixed-type	-41.40	Langmuir	[S10]
castor oil-based corrosion inhibitor (COCI)	140 µM	Mild steel	1 M HCl	PDP	60°C	86%	Mixed-type	-41.2	Langmuir	[S11]
Fluconazole	200 ppm	API 5L X52	1 M HCl	EIS	20°C	90.6%	Mixed-type	-23.7	Langmuir	[S12]
1,2,4-trizole	200 ppm	API 5L X52	1 M HCl	EIS	20°C	91.4%	Mixed-type	-18.0	Langmuir	[S12]
1-bromo-2,4-di-fluorobenzene	200 ppm	API 5L X52	1 M HCl	EIS	20°C	82.4%	Mixed-type	-20.8	Langmuir	[S12]
Afungil	200 ppm	API 5L X52	1 M HCl	EIS	20°C	79.1%			Langmuir	[S12]
1-benzyl-4-phenyl-1H-1,2,3-triazole	2.13 mM	A36 mild steel	1 M HCl	Weight-loss	328 K	94.2%	Mixed-type	-35.7	Langmuir	[S13]
Ginkgoleaf extract	200 mg/L	X70 steel	1 M HCl	EIS	318 K	92.5%	Mixed-type	-28.83	Langmuir	[S14]
(4-benzothiazole-2-yl-phenyl)-dimethyl-amine	50 ppm	Mild steel	1 M HCl	Weight-loss	25°C	96.8%	Mixed-type	-40.80	Langmuir	[S15]
(1-benzyl-1H-1,2,3-triazole-4-yl)methanol (BTM)	1 mM	Mild steel	1 M HCl	Weight-loss	25°C	97.8%			Langmuir	[S16]
(1-(pyridin-4-ylmethyl)-1H-1,2,3-triazole-4-yl)methanol (PTM)	1 mM	Mild steel	1 M HCl	Weight-loss	25°C	99.0%			Langmuir	[S16]
Methionine	10 mM	Carbon steel	0.5 M H_2SO_4	EIS	25°C	85.92%				[S17]
2-(4-nitrophenyl) benzimidazole (4NPBI)	1 mM	Mild steel	1 M HCl	PDP	303 K	93.7%	Mixed-type	-39.12	Langmuir	[S18]
2-(4-aminophenyl) benzimidazole (4APBI)	1 mM	Mild steel	1 M HCl	PDP	303 K	89.7%	Mixed-type	-37.94	Langmuir	[S18]
2-(2-nitrophenyl) benzimidazole (2NPBI)	1 mM	Mild steel	1 M HCl	PDP	303 K	87.8%	Mixed-type	-37.32	Langmuir	[S18]
2-(2-aminophenyl) benzimidazole (2APBI)	1 mM	Mild steel	1 M HCl	PDP	303 K	85.0%	Mixed-type	-36.68	Langmuir	[S18]
2-phenyl benzimidazole (PBI)	1 mM	Mild steel	1 M HCl	PDP	303 K	81.3%	Mixed-type	-35.95	Langmuir	[S18]
2-(n-hexylamino)-4-(3'-N,N-dimethylamino-propyl)amino-6-(benzothiazol-2-yl)thio-1,3,5-s-triazine (BTC6T)	1 mM	Carbon steel	1 M HCl	Weight-loss	40°C	92.3%	Mixed-type	-36.52	Langmuir	[S19]
2-(n-octylamino)-4-(3'-N,N-dimethylamino-propyl)amino-6-(benzothiazol-2-yl)thio-1,3,5-s-triazine (BTC8T)	1 mM	Carbon steel	1 M HCl	Weight-loss	40°C	92.9%	Mixed-type	-37.92	Langmuir	[S19]
2-((Thiazole-2-ylimino)methyl)phenol (THYMP)	10 mM	Mild steel	2 M HCl	Weight-loss	303 K	94%	Mixed-type	-34.3	Langmuir	[S20]
tetra-n-butylammonium L-methioninate [TBA][L-Met]	1.59 mM	Mild steel	1 M HCl	PDP	°C	95.1%	Mixed-type	-9.9	Frundlich	[S21]
2-amino-5-(3-pyridyl)-1,3,4-thiadiazole(3-APTD)	6 mM	Mild steel	0.5 M H_2SO_4	EIS	30°C	92%		-33.36	Langmuir	[S22]
2-amino-5-(4-pyridyl)-1,3,4-thiadiazole (4-APTD)	6 mM	Mild steel	0.5 M H_2SO_4	EIS	30°C	95%		-33.34	Langmuir	[S22]
5-((E)-4-phenylbuta-1,3-dienylideneamino)-1,3,4-thiadiazole-2-thiol (PDTT)	1 mM	Mild steel	0.5 M HCl	EIS	298 K	97.9%	Mixed-type	-40.16	Langmuir	[S23]
3,4-dihydroxy-L-phenylalanine (L-DOPA)	200 mg/L	Mild steel	1 M HCl	PDP	Room temperature	97.95%	Mixed-type	-30.41	Langmuir	[S24]
xcess sewage sludge (ESS)	0.372 g/L		10% HCl	Weight-loss	°C	93.5%	Mixed-type	-24.52	Langmuir	[S25]
Hexadecylpyridinium bromide (HDPB)	1 mM	Mild steel	0.5 M H_2SO_4	EIS	60°C	91%	Mixed-type	-39.50	Bockris–Swinkels	[S26]
Polyaspartic acid (PASP)	2 g/L	Mild steel	0.5 M H_2SO_4	Weight-loss	303 K	87.9%				[S27]
2-[4-(2-chlorobenzyl)-3-methyl-6-thiooxopyridazin-1(6H)-yl]acetohydrazide	25 mM	Steel	0.5 M H_2SO_4	Weight-loss	298 K	99%		-18.76	Temkin	[S28]
N,N-Diethylammonium O,O'-di(4-bromophenyl)dithiophosphate (Br-NOP)	100 mg/L	Q235 steel	0.5 M H_2SO_4	EIS	300 K	98.07%		-39.61	Langmuir	[S29]
Omeprazole (OMP)	300 mg/L	X60 Steel	0.5 M H_2SO_4	EIS	298 K	92.52%		-26.06	Langmuir	[S30]

Table S6 List of corrosion inhibitors for brass in literature.

Inhibitor	Concentration	Test solution	Method	Temperature	Inhibition efficiency	Mechanism of action	ΔG_{ads} (kJ/mol)	Adsorption isotherm	Reference
Sodium gluconate (SG) and cetyltrimethyl ammonium bromide (CTAB)	10^{-3}M of SG, 5ppm CTAB	0.5 M H_2SO_4	PDP	303K	89%	Cathodic-type	-44.1	Langmuir	[S31]
Polyanethol sulfonate	0.1%	simulated urban rain (pH = 5)	PDP	25℃	90%	Mixed-type			[S32]
4-aminothiophenol (4-ATP)	200ppm	0.5 M HNO_3	PDP	25℃	81%	Cathodic-type	-32.77	Langmuir	[S33]
4-amino phenol disulfide (4-APD)	200ppm	0.5 M HNO_3	PDP	25℃	93%	Cathodic-type	-31.05	Langmuir	[S33]
natural extract ofCamellia sinensis	1 g/L	0.1 M Na_2SO_4(pH = 4)	EIS	Room temperature	95%	Mixed-type			[S34]
Mimosa extract	2000ppm	0.5 M H_2SO_4	PDP EIS	Room temperature	63.5% 60.24%	Anodic-type	-6.0138	Temkin	[S35]
1-diethylamino-propan-2-ol (EAP)	0.01 mol/L	simulatedatmospheric water	EIS		90.7%	Anodic-type			[S36]
1,3-bis-diethylamino-propan-2-ol (DEAP)	0.01 mol/L	simulatedatmospheric water	EIS		92.9%	Anodic-type			[S36]
1,3-bis-diethylamino-propan-2-ol (DEAP)	10 mM	simulatedatmospheric water	Weight-loss	50℃	94.3%	Anodic-type		Langmuir	[S37]
N-[1-(benzotriazol-1-yl)ethyl]aniline (BTEA)	150 ppm	3% NaCl solution	Weight-losst	Room temperature	~88%	Mixed-type			[S38]
N,N-dibenzotriazol-1-ylmethylaminoethane (DBME)	150 ppm	3% NaCl solution	Weight-loss	Room temperature	~92%	Mixed-type			[S38]
Benzotriazole(BTA)	150 ppm	3% NaCl solution	Weight-loss	Room temperature	74.80%	Mixed-type			[S39]
N-[1-(benzotriazol-1-yl)methyl]aniline (BTMA)	150 ppm	3% NaCl solution	Weight-loss	Room temperature	85.08%	Mixed-type			[S39]
1-hydroxy methyl benzotriazole (HBTA)	150 ppm	3% NaCl solution	Weight-loss	Room temperature	91.13%	Mixed-type			[S39]
Gluconic acid sodium (GASS)	0.01 M	3% NaCl solution	EIS		~95%				[S40]
Polyphosphoric acid sodium salt (PP)	1 g/L	3% NaCl solution	EIS		~50%				[S40]

8. Grand Canonical Monte Carlo (GCMC) Calculations

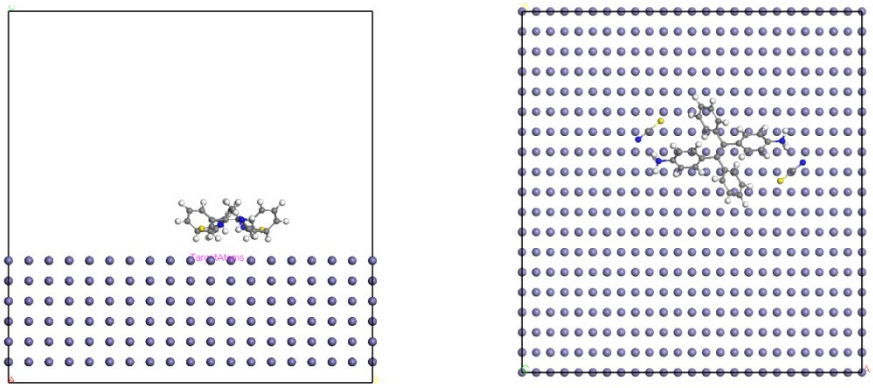

Fig. S49 Side view (left) and top view (right) of equilibrium adsorption configuration for TPE-$2NH_3{\cdot}2SCN$ on steel obtained by GCMC simulation in solution.

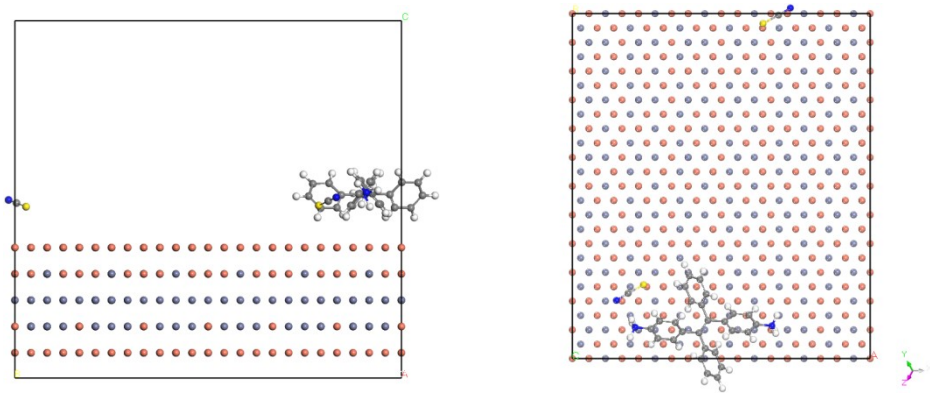

Fig. S50 Side view (left) and top view (right) of equilibrium adsorption configuration for TPE-$2NH_3{\cdot}2SCN$ on brass obtained by GCMC simulation in solution.

Reference:

[S1] J. Xiong, W. Xie, J. Sun, J. Wang, Z. Zhu, H. Feng, D. Guo, H. Zhang and Y. Zheng, J. *Org. Chem.*, 2016, **81**, 3720-3726.

[S2] A. Schreivogel, J. Maurer, R. Winter, A. Baro and S. Laschat, *Eur. J. Org. Chem.*, 2006, 3395-3404.

[S3] J. Lu and J. Zhang, *J. Mater. Chem. A*, 2014, **2**, 13831-13834.

[S4] T. Yu, D. Ou, Z. Yang, Q. Huang, Z. Mao, J. Chen, Y. Zhang, S. Liu, J. Xu, M.R. Bryce and Z. Chi, *Chem. Sci.*, 2017, **8**, 1163-1168.

[S5] W. Zhao, Z. He, Q. Peng, J. W. Y. Lam, H. Ma, Z. Qiu, Y. Chen, Z. Zhao, Z. Shuai, Y. Dong and B. Z. Tang, *Nat. Commun.*, 2018, **9**, 3044-3051.

[S6] T. Zheng, J. Liu, M. Wang, L. Qian, J. Wang, Y. Chong and G. Lia, *Corros. Sci.*, 2022, 199, 110199.

[S7] K. Dharmendr, K. Venkata Muralidhar, J. Vinay and R. Beena, *Corros. Sci.*, 2022, **208**, 110623.

[S8] K. Kousar, M. S. Walczak, T. Ljungdahl, A. Wetzel, H. Oskarsson, P. Restuccia, E. A. Ahmad, N. M. Harrison and R. Lindsay, *Corros. Sci.*, 2021, **180**, 109195.

[S9] A. L. Paulina, D. J. Víctor, H. Hernández-Cocoletzi, N. Noel, O. X. Octavio and V. L. Natalya, *Corros. Sci.*, 2020, **175**, 108888.

[S10] J. Haque, V. Srivastava, M. A. Quraishi, D. Singh Chauhan, H. Lgaz and I. Chung, *Corros. Sci.*, 2020, 172, 108665.

[S11] A. Farhadian, A. Rahimi, N. Safaei, A. Shaabani, M. Abdouss and A. Alavi, *Corros. Sci.*, 2020, **175**, 108871.

[S12] A. Espinoza-Vázquez, F. J. Rodríguez-Gómez, G. E. Negrón-Silva, R. González-Olvera, D. Ángeles-Beltrán, M. Palomar-Pardavé, A. Miralrio and M. Castro, *Corros. Sci.*, 2020, **174**, 108853.

[S13] F. Caio Machado, X. A. Leonardo, S. Nazir Escarpini dos, C. M. B. Adriana and P. Eduardo Ariel, *Corros. Sci.*, 2019, **149**, 185-194.

[S14] Y. Qiang, S. Zhang, B. Tan and S. Chen, *Corros. Sci.*, 2018, **133**, 6-16.

[S15] S. Zohreh, A. Mehdi, T. Milad, R. Keyvan and M. Soraia, *Corros. Sci.*, 2017, **114**, 133-145.

[S16] M. Qi, Q. Sijun, H. Xiaohong, T. Yongming and L. Gang, *Corros. Sci.*, 2017, **129**, 91-101.

[S17] L. F. M. Glaydson, N. C. Stefane, N. F. Valder, N. S. C. Paulo, N. C. Adriana and L.-N. Pedro de, *Corros. Sci.*, 2017, **115**, 41-55.

[S18] A. Dutta, S. K. Saha, U. Adhikari, P. Banerjee and D. Sukul, *Corros. Sci.*, 2017, **123**, 256-266.

[S19] Z. Hu, Y. Meng, X. Ma, H. Zhu, J. Li, C. Li and D. Cao, *Corros. Sci.*, 2016, **112**, 563-575.

[S20] Y. Nurdane, F. Alper, E. ÿmit and C.E. Kaan, *Corros. Sci.*, 2016, **111**, 110-120.

[S21] E. Kowsari, S. Y. Arman, M. H. Shahini, H. Zandi, A. Ehsani, R. Naderi, A. PourghasemiHanza and M. Mehdipour, *Corros. Sci.*, 2016, **112**, 73-85.

[S22] Y. Tang, X. Yang, W. Yang, R. Wan, Y. Chen and X. Yin, *Corros. Sci.*, 2010, **52.5**, 1801-1808.

[S23] R. Solmaz, *Corros. Sci.*, 2010, **52.10**, 3321-3330.

[S24] H. Zhao, T. Sun, L. Huang, J. Wei and S. Qiu, *Chem. Eng. J.*, 2022, **437**, 135242.

[S25] W. Su, B. Tang, F. Fu, S. Huang, S. Zhao, L. Bin, J. Ding and C. Chen, *J. Hazard. Mater.*, 2014, **279**, 38-45.

[S26] Mahmoud M. Saleh, *Mater. Chem. Phys.*, 2006, **98**, 0254-0584.

[S27] B. Qian, J. Wang, M. Zheng and B. Hou, *Corros. Sci.*, 2013, **75**, 0010-938X.

[S28] M. Bouklah, N. Benchat, A. Aouniti, B. Hammouti, M. Benkaddour, M. Lagrenée, H. Vezin and F. Bentiss, *Prog. Org. Coat.*, 2004, **51**, 0300-9440.

[S29] C. Lai, X. Su, T. Jiang, L. Zhou, B. Xie, Y. Li and L. Zou. *Int. J. Electrochem. Sci.*, 2016, **11**, 9413-9423.

[S30] Y. Liu, W. Du, X. Yao, C. Liu, X. Luo, L. Guo and C. Guo, *Int. J. Electrochem. Sci.*, 2022, **17**, 220516.

[S31] J. Jennane, M. Ebn Touhami, S. Zehra, Y. Baymou, S. Kim, I. Chung, and H. Lgaz, *Mater. Chem. Phys.*, 2019, **227**, 200.

[S32] R. Fuchs-Godec, *J. Mol. Liq.*, 2017, **228**, 230.

[S33] M. Ebrahimzadeh, M. Gholami, M. Momeni, A. Kosari, M. H. Moayed and A. Davoodi, *Appl. Surf. Sci.*, 2015, **332**, 384.

[S34] R. Tambi, R. Stefano and Z. Caterina, *Appl. Surf. Sci.*, 2014, **307**, 209.

[S35] H. Gerengi, K. Schaefer and H. I. Sahin, *J. Ind. Eng. Chem.*, 2012, **18**, 2204.

[S36] G. Guo and L. Chenghao, *Electrochim. Acta*, 2007, **52**, 4554.

[S37] G. Gao and C. Liang, *Corros. Sci*., 2007, **49**, 3479.

[S38] R. Ravichandran and N. Rajendran, *Appl. Surf. Sci.*, 2005, **239**, 182.

[S39] R. Ravichandran, S. Nanjundan and N. Rajendran, *Appl. Surf. Sci.*, 2004, **236**, 241.

[S40] A. Nagiub and F. Mansfeld, *Corros. Sci.*, 2001, **43**, 2147.